Copy

RM A55D18

NACA RM A55D18

NACA

RESEARCH MEMORANDUM

A FLIGHT INVESTIGATION AT TRANSONIC SPEEDS OF A MODEL HAVING A TRIANGULAR WING OF ASPECT RATIO 3

By Maurice D. White

Ames Aeronautical Laboratory
Moffett Field, Calif.

NATIONAL ADVISORY COMMITTEE
FOR AERONAUTICS

WASHINGTON
June 24, 1955
Declassified April 8, 1957

NATIONAL ADVISORY COMMITTEE FOR AERONAUTICS

RESEARCH MEMORANDUM

A FLIGHT INVESTIGATION AT TRANSONIC SPEEDS OF A MODEL HAVING A TRIANGULAR WING OF ASPECT RATIO 3

By Maurice D. White

SUMMARY

Free-falling recoverable-model tests were conducted at transonic speeds on a model having a triangular wing of aspect ratio 3 and a 45° swept tail located in the chord plane of the wing. Static and dynamic longitudinal-stability data for the complete model, force and moment data for the major components of the model, and load distributions over the fuselage of the model were evaluated at angles of attack up to about 16° to 22°, depending on the Mach number. The drag-rise-with-lift factor for the wing was found to decrease with increasing Mach number and simultaneously increasing Reynolds number, through the transonic Mach number range covered by the tests. For low lift coefficients the transonic variation of aerodynamic-center position for the complete model was about 13 percent of the mean aerodynamic chord. A large variation of downwash angle with angle of attack was indicated at small angles of attack similar to that reported in other tests of low-aspect-ratio wings with tail locations in the wing chord plane. Buffeting of the model was experienced at angles of attack greater than about 7° between Mach numbers of 0.96 and 1.08.

INTRODUCTION

As part of a general investigation of the characteristics of low-aspect-ratio wings, flight tests were conducted on a model having a triangular wing of aspect ratio 3 with an NACA 0005-63 airfoil section and a 45° swept horizontal tail. The flight tests of the same fuselage-tail combination with other wings were reported in references 1, 2, and 3. The wing of reference 3 differed from that reported on here only in aspect ratio. Wings of the same plan form as the wing of the present tests, but not necessarily the same airfoil section, have been tested in other NACA facilities (see, for example, refs. 4, 5, 6, and 7). In the present tests the ranges of the wind-tunnel investigations were extended in the following particulars:

1. The tests were made at higher Reynolds numbers (8 million to 22 million) at transonic Mach numbers (M = 0.80 to 1.12).

2. Dynamic as well as static longitudinal-stability characteristics of the model were obtained.

3. Loading distributions over the fuselage of the model were obtained.

4. Aerodynamic forces and moments were evaluated for the complete model, as well as for the major components of the model, the wing, the fuselage, and, by taking differences, the tail.

The tests were made by the Ames Aeronautical Laboratory using the free-falling recoverable-model technique in an area provided by the Air Force at Edwards Air Force Base, Edwards, California.

SYMBOLS

A	aspect ratio
b	wing span, ft
c	local chord, ft
$\bar{c}$	mean aerodynamic chord of the wing, $\frac{2}{S}\int_0^{b/2} c^2 dy$, ft
I_y	moment of inertia of the model about the Y axis, slug-ft^2
M	Mach number
p	static pressure at a fuselage orifice, lb/sq ft
ΔP	$\frac{p_l - p_u}{q_o}$
q	rate of pitch, radians/sec
q_o	dynamic pressure, lb/sq ft
$\dot{q}$	angular acceleration in pitch, radians/sec^2
R	Reynolds number
r	radius of fuselage at longitudinal station x, in.

S wing area, including portion of wing covered by fuselage, sq ft

V speed, ft/sec

x longitudinal distance from fuselage station 0, in.

y spanwise distance from model center line, ft

C_D drag coefficient, $\frac{\text{drag}}{q_o S}$

C_L lift coefficient, $\frac{\text{lift}}{q_o S}$

C_m pitching-moment coefficient, $\frac{\text{pitching moment}}{q_o S \bar{c}}$

C_{m_q} $\frac{\partial C_m}{\partial\left(\frac{q\bar{c}}{2V}\right)}$

$C_{m_{\dot{\alpha}}}$ $\frac{\partial C_m}{\partial\left(\frac{\dot{\alpha}\bar{c}}{2V}\right)}$

α angle of attack, deg

$\dot{\alpha}$ rate of change of angle of attack, radians/sec

δ deflection of horizontal tail, deg

ϵ downwash angle, deg

Subscripts

e exposed panels

l lower

T complete model

t horizontal tail

u upper

w total wing

max maximum

min minimum

α,δ derivative of the factor with respect to the subscript, as $C_{L_\alpha} = \frac{\partial C_L}{\partial \alpha}$, etc.

MODEL

A three-view drawing of the complete model is shown in figure 1 and additional pertinent dimensions are listed in table I. Figure 2 is a photograph of the model taken immediately after release from the carrier airplane. Shown attached to the model in figure 2 is the booster which was used in some of the tests to obtain higher Mach numbers.

The wing was of triangular plan form with an aspect ratio of 3. The airfoil section was the NACA 0005-63 parallel to the free stream; ordinates of this airfoil section are listed in table II. The wing panels were constructed with a composite steel core and a plastic covering, the whole covered with plastic-impregnated glass cloth. The juncture of the wing root and the fuselage was sealed with a flexible rubber seal.

All other components of the model were as described in reference 8.

INSTRUMENTATION

Forces and moments on the exposed wing panels were measured on internal strain-gage balances. Forces and moments on the complete model were determined by accelerometer measurements. The instrumentation was identical to that described in reference 1 except that potentiometers were substituted for selsyns as transducers for the angle of attack and the angle of sideslip.

TESTS

The test procedure used was the same as that described in references 8 and 9; that is, the model was released from the carrier airplane at high altitude and allowed to accelerate in free fall. After the test Mach number was attained, the horizontal control was pulsed intermittently, and data were recorded during the ensuing control-fixed oscillations. At the conclusion of the test run, the model was decelerated

by opening a dive brake, and was finally eased to the ground on a parachute. For some drops, rocket assist was employed in order to increase the attainable Mach number. The booster rocket (fig. 2) was jettisoned at the conclusion of boost and prior to the actual test period.

The Mach numbers of the tests ranged from 0.80 to 1.12, the Reynolds numbers from 8 million to 22 million (fig. 3), and the angles of attack from -1° to 22° for Mach numbers less than about 0.95, and from -1° to 16° for Mach numbers greater than 0.95. The center of gravity was located at $0.299\bar{c}$ or $0.397\bar{c}$, depending on the drop.

Data are presented in this report for five settings of the horizontal tail. Each horizontal-tail angle is identified with a different trim angle-of-attack curve in figure 4.

The model was recovered at the conclusion of one drop with a 1/4-inch-thick portion of the covering of one wing panel broken out as shown in figure 5; the particular drop is identified in figure 4 as $\delta = -12\text{-}1/2^{\circ}$. The flight records gave no indication of the time that the failure occurred, leaving open the possibility that it occurred subsequent to the test phase of the drop. Since, in addition, there were no serious discrepancies between the data from this drop and adjacent data from other drops, these data were treated as though the wing were undamaged.

PRECISION OF MEASUREMENT

The range and accuracy of the instruments used in the present investigation were such as to give the same accuracy as was obtained in the investigation of reference 8. It follows then that the error of any single quantity will for most of the coefficients be equal to the values given in reference 8, as follows:

Item	Estimated maximum error	
	$M = 0.85$	$M = 1.05$
Mach number	±0.01	±0.01
angle of attack	$\pm 1/4^{\circ}$	$\pm 1/4^{\circ}$
C_{L_T}	±.02	±.009
C_{L_e} and C_{L_w}	±.02	±.008
C_{D_T}	±.002	±.001
C_{D_e} and C_{D_w}	±.006	±.002
C_{m_T}	±.001	±.001
$\left(C_{m_{\bar{c}/4}}\right)_e$ and $\left(C_{m_{\bar{c}/4}}\right)_w$	±.005	±.002

For one drop, that identified in figure 4 as $\delta = -9\text{-}1/2^{\circ}$ and $-15\text{-}1/2^{\circ}$, the vertical acceleration record was lost and was estimated on the basis of the wing lift. For this drop, errors in estimation might have been as great as 10 percent. The corresponding errors in the coefficients C_{L_T} and C_{D_T}, would be 10 percent. Because this error affects only the inertia loads of the wing panels, the corresponding errors in the coefficients C_{L_e}, C_{L_w}, C_{D_e}, and C_{D_w} would be much smaller, of the order of 2 percent. The error in $\left(C_{m_{\bar{c}/4}}\right)_e$ and $\left(C_{m_{\bar{c}/4}}\right)_w$ additional to those previously listed would be of the order of ±0.003.

The over-all accuracy of the final results is, of course, a function of factors additional to the precision of the instruments, but to which it is difficult to assign quantitative values. For example, the accuracy of any one "static" data point is reduced by the fact that it is determined through time correlation of a number of rapidly varying records. However, in deriving the curves showing the variation of a "static" quantity with, say, angle of attack, a large volume of data points is considered, which helps to define more closely the correct fairing of the data. Also, shifts in the data which occurred from drop to drop were usually definable to a close degree by reference to a number of different records, and by the fact that the entire configuration was symmetrical with control undeflected. Consideration of all these factors leads to the conclusion that the accuracy of "static" results which were obtained by fairing the flight data is of the order of the values listed above.

RESULTS

In general, the flight data were evaluated by the methods described in references 8 and 9. The results are identified as applying to the following:

1. The exposed wing panels.

2. The total wing, obtained by adding to the data for the exposed wing panels, the data obtained by integrating the pressure differences over the fuselage between stations 51 and 135. An additional total-wing drag increment was obtained by applying a skin-friction coefficient of 0.0028 to the entire fuselage surface area between stations 51 and 135.

3. The complete model.

Lift

In figure 6 curves are presented of C_L against α for the test Mach number range, and in figure 7 the lift-curve slopes for the various components are plotted as a function of Mach number. In presenting the lift-curve slopes for the complete model in figure 7, it was assumed that the slopes were unaffected by deflections of the horizontal tail.

Drag

Curves of C_D against C_L for the various components are plotted in figure 8 for various Mach numbers. In figures 9(a), 9(b), and 9(c) are plotted, respectively, as a function of Mach number, the values of $C_{D_{min}}$ for the total wing and the complete model, the values of the drag-rise factor $\partial C_D/\partial C_L^2$ for the total wing, and the values of the $\partial C_D/\partial C_L^2$ for the exposed wing. The curves of C_D against C_L^2 from which these values were obtained were linear up to, and in some cases beyond, the value of C_L of 0.25 which is indicated in figures 9(b) and 9(c) to be the limit of applicability of the data. There were insufficient data with the control undeflected to permit evaluation of the factor $\partial C_D/\partial C_L^2$ for the complete model.

Static Longitudinal Stability

The variation of trim angle of attack with Mach number for several horizontal-tail positions is shown in figure 4.

In figure 10(a) is shown the variation with angle of attack of C_{m_T} as determined from $C_{m_T} = I_y\dot{q}/q_oS\bar{c}$, using the data evaluation procedures described in reference 8. A slight departure from the method of reference 8 was made in that the small effects of pitch damping were eliminated by fairing between values for positive and negative pitching velocities rather than by calculating the magnitudes of the damping contribution. Also shown in figure 10(a) are straight lines having the slope $C_{m_{\alpha_T}}$ as determined from the periods of the control-fixed oscillations. For clarity of presentation the lines are drawn displaced in C_m from their actual locations by arbitrary amounts. No lines for $C_{m_{\alpha_T}}$ are shown for the drop defined in figure 4 by $\delta = -9\text{-}1/2^\circ$ to $-15\text{-}1/2^\circ$, because the oscillations were not regular enough to give a well-defined period in the presence of the stalling that occurred in that drop.

Curves of C_{m_T} against α have been calculated for $\delta = 0^{\circ}$ for a center-of-gravity location of $0.25\bar{c}$ for the complete angle-of-attack ranges covered by the tests by applying corrections to the data of figure 10(a) for differences in center-of-gravity location and in horizontal-tail setting. The calculated curves are presented in figure 10(b) together with corresponding curves for the exposed wing panels and the total wing. The pitching-moment coefficients due to the tail with $\delta = 0^{\circ}$, as determined by subtracting from the total-model data the data for the total wing, are also included in figure 10(b). By this method of evaluation the value of C_{m_t} will include the contribution to C_m of the portion of the fuselage forward of the region where pressures are measured. The magnitude of this contribution is believed to be inconsequential in relation to that of the tail.

The wing pitching moments about the wing quarter-chord point have been cross-plotted in figure 11 in terms of C_{m_e} against C_{L_e}, and C_{m_w} against C_{L_w}. The variations with Mach number of the aerodynamic-center location for various components of the model at small angles of attack are shown in figure 12.

Dynamic Longitudinal Stability

Values of $C_{m_q} + C_{m_{\dot{\alpha}}}$ for the complete model are shown in figure 13 as a function of Mach number. These values were obtained in the usual manner; that is, by deducting the contribution of the lift-curve slope from the total damping factor that was obtained from analysis of the control-fixed oscillations of the model.

Horizontal-Tail Effectiveness

The variation with Mach number of the horizontal-tail effectiveness parameter C_{m_δ} is shown in figure 14. Two methods were used to evaluate this parameter. One method was to plot C_{m_T} against δ during a control pulse, selecting data only for regimes where α was reasonably constant. The second method used was to plot as a function of $\Delta\delta_{trim}$ the change in C_{m_T} that would be required to aline the curves of figure 10(a) for $\delta \neq 0^{\circ}$ with those for $\delta = 0^{\circ}$.

Loading Distribution Over Fuselage

In figure 15 are plotted the distributions of loading along the fuselage center line and along a line displaced 45° from the center line.

The locations of the orifices from which the data were obtained are shown in figure 16. The data represent the difference in pressure coefficient between corresponding orifices on the top and bottom of the fuselage.

Buffet Boundary

Figure 17 shows the variation with Mach number of the angle of attack at which buffeting began. These data were obtained from two of the drops; in the remaining drops the angle of attack was either below or above the boundary throughout the drop. The results indicate that buffeting was experienced at angle of attack greater than about 7° for Mach numbers between 0.96 and 1.08.

DISCUSSION

Lift

The lift curves of figure 6 show fairly regular variations with angle of attack up to the maximum lift coefficient or to the maximum test angle of attack, whichever occurred first. The lift-curve slopes at small angles of attack for the total wing and for the complete model (fig. 7) are compared, respectively, in figures 18(a) and 18(b) with values obtained in other facilities for wings of the same plan form (refs. 4, 5, 6, 7, 10, 11, and 12). The comparisons indicate good agreement with data from the Ames 12-foot and 6- by 6-foot wind tunnels, and the Langley Pilotless Aircraft Research Division. The data from the Ames 2- by 2-foot wind tunnel are in agreement over parts of the Mach number range, while the data from the Ames 16-foot wind-tunnel bump, and the Langley 26-inch transonic blowdown tunnel show considerably lower slopes. Comparisons of test conditions indicate that the lower lift-curve slopes of the latter tests are not due to differences in Reynolds number or in airfoil thickness. In the absence of other explanations, nonuniformities of tunnel air flow appear to be a likely cause of the discrepancies.

The lift curves for the wing generally decrease in slope with increasing angle of attack (figs. 6 and 7). This trend is exhibited by the wind-tunnel data also.

For Mach numbers less than about 0.92 the maximum lift of the total wing occurs at about 17° angle of attack. The value of the maximum lift coefficient increases from 0.85 to 0.97 as the Mach number increases from 0.84 to 0.92. Some irregularities are apparent in the lift curves at angles of attack less than that for maximum lift. Such irregularities are frequently associated with undesirable stalling characteristics which could limit the usable lift coefficients of this wing to values less than

the maximum quoted above. For Mach numbers greater than 0.96, the maximum lift coefficient was not attained at the highest test angle of attack of 16°.

Drag

In figure 9(a) the flight variation of minimum drag coefficient with Mach number for the complete model is compared with the theoretical variation computed by adding to the subsonic value the increment determined by the method described in reference 13. The computed and flight curves are seen to be in excellent agreement with each other.

In figures 9(b) and 9(c) the experimental curves of drag rise with lift, expressed in terms of the factor $\partial C_D/\partial C_L^2$, are compared with values computed assuming (1) an elliptic spanwise distribution of lift at subsonic speeds $(1/\pi A)$, with modifications according to linear theory for Mach numbers greater than 1.0; and (2) the resultant-force vector due to angle of attack perpendicular to the wing chord $(1/57.3\ C_{L_\alpha})$. Low-lift values of C_{L_α} were used in the expression $1/57.3\ C_{L_\alpha}$. The results show a large and generally progressive variation with Mach number through the test range. At a Mach number of 0.88 the resultant-force vector due to angle of attack is inclined only a moderate amount from perpendicularity to the chord, but as the Mach number is increased the drag-rise factor approaches the minimum values given by linear theory. This variation is different from that experienced with the unswept wing of reference 1 and the aspect-ratio-4 triangular wing of reference 3.

Reference 14 shows the considerable effect that Reynolds number may have on the value of $\partial C_D/\partial C_L^2$, the value decreasing with increasing Reynolds number at any particular Mach number. In the present tests the Reynolds number varied simultaneously with the Mach number in each drop. The particular variation for the drop that defined the curves of $C_{D_{min}}$ and $\partial C_D/\partial C_L^2$ is shown as a supplementary scale in figure 9. Because of this simultaneous variation it is impossible from these tests to state with certainty whether Mach number or Reynolds number is the determining factor.

Static Longitudinal Stability

In figures 19(a) and 19(b) the variation of aerodynamic-center location with Mach number at low lift coefficients as determined from the flight tests is compared with the variations measured for wings of the same plan form in other test facilities (refs. 4, 11, 12, and 15). The variations are similar, the aerodynamic-center movements over the

transonic range being about $0.10\bar{c}$ for the wing and about $0.13\bar{c}$ for the complete model. The absolute aerodynamic-center locations are generally, however, several percent mean aerodynamic chord aft of the locations measured in the other tests.

There was little movement of the aerodynamic center with changing angle of attack over the unstalled range of angles as indicated by the linearity of the curves of figures 10 and 11, and by the small difference in aerodynamic-center location between $\alpha = 0^{\circ}$ and $\alpha = 10^{\circ}$ in figure 12.

At subsonic Mach numbers the stability contribution of the tail was small at small angles of attack (figs. 10(b) and 12). In particular, at a Mach number of 0.92, the tail contribution is indicated to be very small, and even negative at times, over the entire range of angles of attack tested, $\alpha = 0^{\circ}$ to 22°. The tail-effectiveness data of figure 14 do not show sufficient reduction at small angles of attack to account for the stability changes noted. The probable cause of the reduced tail contribution is a large variation of downwash angle with angle of attack. References 4 and 6 both show large variations of downwash angle with angle of attack at small angles of attack for Mach numbers and tail locations corresponding to the tests of this report. These same references also show that at Mach numbers in the vicinity of 0.92, the large downwash-angle variations persist to the highest angles of attack of any of the Mach numbers covered by the two investigations. Similar indications of large downwash-angle variations at small angles of attack were also reported for tails located in the chord planes of two other low-aspect-ratio wing plan forms (refs. 1 and 3). It seems fairly well established from all these results that, at least for operation at high subsonic Mach numbers, a tail located near the chord plane of low-aspect-ratio wings will contribute little to the static stability.

Dynamic Longitudinal Stability

The results of figure 13 show that values of the damping-in-pitch parameter $C_{m_q} + C_{m_{\dot{\alpha}}}$ are of the same order as values estimated for the fuselage plus the tail in the presence of the wing. The contribution of the tail was estimated as described in reference 9 using a value of $\partial\epsilon/\partial\alpha$ of 0.5. In view of the preceding discussion that indicated the existence of much higher values of $\partial\epsilon/\partial\alpha$ at small angles of attack, a higher value of $\partial\epsilon/\partial\alpha$ should probably have been used in the calculation. However, further refinements of this kind were considered unwarranted in view of the nonlinearity of the variation of ϵ with α and the fact that each value of $C_{m_q} + C_{m_{\dot{\alpha}}}$ was determined from several cycles of data, each of which covered a different range of angles of attack.

Some values of $C_{m_q} + C_{m_{\dot{\alpha}}}$ are shown in reference 16 for a wing of the same plan form as the test wing. Addition of the increment for the wing as obtained from reference 16 to the estimated values for the fuselage and tail seems to improve the agreement with the flight data in figure 13; this agreement should, however, be regarded as fortuitous in view of the nonlinearities previously discussed.

Horizontal-Tail Effectiveness

In figure 14 flight values of the parameter C_{m_δ} are compared with other flight data for the same tail located behind wings of other plan form. In general, the results appear to be consistent with the previous data.

SUMMARY OF RESULTS

Flight tests at transonic speeds of a free-falling model incorporating an aspect-ratio-3 triangular wing and a 45° swept horizontal tail in the chord plane of the wing showed the following results:

1. The drag-rise-with-lift factor for the wing decreased with increasing Mach number and simultaneously increasing Reynolds number throughout the transonic speed range. This result contrasts with previously obtained flight results on an unswept wing and an aspect-ratio-4 triangular wing which showed little variation in the factor throughout the same range of Mach numbers.

2. A large variation of downwash angle with angle of attack at small angles of attack that had been reported in other tests with tail locations in the chord plane of low-aspect-ratio wings was also indicated in the present investigation. The range of angles of attack over which this effect was observed was particularly large at Mach numbers near 0.92.

3. For low lift coefficients the transonic variations of aerodynamic-center position for the complete model was about 13 percent of the mean aerodynamic chord.

4. Buffeting of the model was experienced at angles of attack greater than about 7° at Mach numbers between 0.96 and 1.08.

5. The lift characteristics of the model were similar to those determined in other tests of wings of the same plan form.

Ames Aeronautical Laboratory
National Advisory Committee for Aeronautics
Moffett Field, Calif., Apr. 18, 1955

REFERENCES

1. White, Maurice D.: A Flight Investigation at Transonic Speeds of the Aerodynamic Characteristics of a Model Having a Thin Unswept Wing of Aspect Ratio 3.1. NACA RM A54E12, 1954.

2. Holdaway, George H.: A Flight Investigation at Transonic Speeds and Small Angles of Attack of the Aerodynamic Characteristics of a Model Having a 45° Sweptback Wing of Aspect Ratio 3 With an NACA 64A006 Airfoil Section. NACA RM A54I17, 1955.

3. Bright, Loren G.: A Flight Investigation at Transonic Speeds of a Model Having a Triangular Wing of Aspect Ratio 4. NACA RM A54L27, 1955.

4. Tinling, Bruce E., and Lopez, Armando E.: The Effects of Horizontal-Tail Location and Size on the Subsonic Longitudinal Aerodynamic Characteristics of an Airplane Model Having a Triangular Wing of Aspect Ratio 3. NACA RM A53L15, 1954.

5. Heitmeyer, John C.: Effect of Vertical Position of the Wing on the Aerodynamic Characteristics of Three Wing-Body Combinations. NACA RM A52L15a, 1953.

6. Axelson, John A.: Downwash Behind a Triangular Wing of Aspect Ratio 3 - Transonic Bump Method. NACA RM A53I23, 1953.

7. Burrows, Dale L., and Palmer, William E.: A Transonic Wind-Tunnel Investigation of the Longitudinal Force and Moment Characteristics of a Plane and a Cambered Three-Percent-Thick Delta Wing of Aspect Ratio 3 on a Slender Body. NACA RM L54H25, 1954.

8. Holdaway, George H.: Comparison of the Aerodynamic Characteristics at Transonic Speeds of a Plane Wing and a Cambered and Twisted Wing, Both Having 45° of Sweepback and an Aspect Ratio of 6. NACA RM A53B16, 1953.

9. White, Maurice D.: Effect of Camber and Twist on the Stability Characteristics of Models Having a 45° Swept Wing as Determined by the Free-Fall Method at Transonic Speeds. NACA RM A52F16, 1952.

10. Emerson, Horace F., and Gale, Bernard M.: Transonic Aerodynamic Characteristics of Three Thin Triangular Wings and a Trapezoidal Wing, All of Low Aspect Ratio. NACA RM A52D21, 1952.

11. Knechtel, Earl D., and Summers, James L.: Effects of Sweep and Taper Ratio on the Longitudinal Characteristics of an Aspect Ratio 3 Wing-Body Combination at Mach Numbers from 0.6 to 1.4. NACA RM A55A03, 1955.

12. Kehlet, Alan B.: Aerodynamic Characteristics at Transonic and Supersonic Speeds of a Rocket-Propelled Airplane Configuration Having a 52.5° Delta Wing and a Low, Swept Horizontal Tail. NACA RM L54A20, 1954.

13. Holdaway, George H.: Comparison of Theoretical and Experimental Zero-Lift Drag-Rise Characteristics of Wing-Body-Tail Combinations Near the Speed of Sound. NACA RM A53H17, 1953.

14. Polhamus, Edward C.: Drag Due to Lift at Mach Numbers up to 2.0. NACA RM L53I22b, 1953.

15. Hall, Charles F.: Lift, Drag, and Pitching Moment of Low-Aspect-Ratio Wings at Subsonic and Supersonic Speeds. NACA RM A53A30, 1953.

16. Tobak, Murray: Damping in Pitch of Low-Aspect-Ratio Wings at Subsonic and Supersonic Speeds. NACA RM A52L04a, 1953.

TABLE I.- DIMENSIONS OF FREE-FALL MODEL

Gross weight, lb	1838 and 1702
Moment of inertia about Y axis, slugs-ft^2	980 and 850
Center of gravity	0.299 and 0.397$\bar{c}$
Wing	
Area, sq ft	31.4
Area, exposed panels, sq ft	23.5
Aspect ratio	3.0
Taper ratio	0
Span, ft	9.71
Mean aerodynamic chord, ft	4.31
Airfoil section, parallel to stream	NACA 0005-63
Horizontal tail (all-movable, pivoting about axis perpendicular to longitudinal axis of model)	
Area (including 2.0 sq ft included in fuselage), sq ft	6.0
Aspect ratio	4.5
Taper ratio	0.20
Span, ft	5.21
Mean aerodynamic chord (including area included in fuselage), ft	1.36
Leading edge of mean aerodynamic chord	Station 153.6
Root chord, ft	1.96
Tip chord, ft	0.40
Airfoil section, parallel to stream	NACA 65006
Gap between tail and fuselage at 0° deflection, in.	1/16
Vertical tail (all-movable differentially, pivoting about axis perpendicular to longitudinal axis of model)	
Area (including 1.4 sq ft included in fuselage) sq ft	3.3
Aspect ratio	5.1
Taper ratio	0.22
Span, ft	4.1
Mean aerodynamic chord (including area included in fuselage), ft	0.93
Leading edge of mean aerodynamic chord	Station 151.0
Root chord, ft	1.34
Tip chord, ft	0.29
Airfoil section, perpendicular to quarter-chord line	NACA 65009
Gap between tail and fuselage at 0° deflection, in.	1/16
Fuselage	
Fineness ratio	12.4
Ordinate at station x (x = 8.0 to x = 139.4), in.	$r = 8.5\left[1 - \left(\frac{x-102}{102}\right)^2\right]^{3/4}$

TABLE II.- ORDINATES OF WING AIRFOIL SECTION

Station, percent chord	Ordinate, percent chord
0	0
1.25	.789
2.50	1.089
5.00	1.481
7.50	1.750
10.00	1.951
15.00	2.227
20.00	2.391
25.00	2.476
30.00	2.501
40.00	2.418
50.00	2.206
60.00	1.902
70.00	1.527
80.00	1.093
90.00	.603
95.00	.336
100.00	.052
Leading-edge radius:	0.278 percent chord

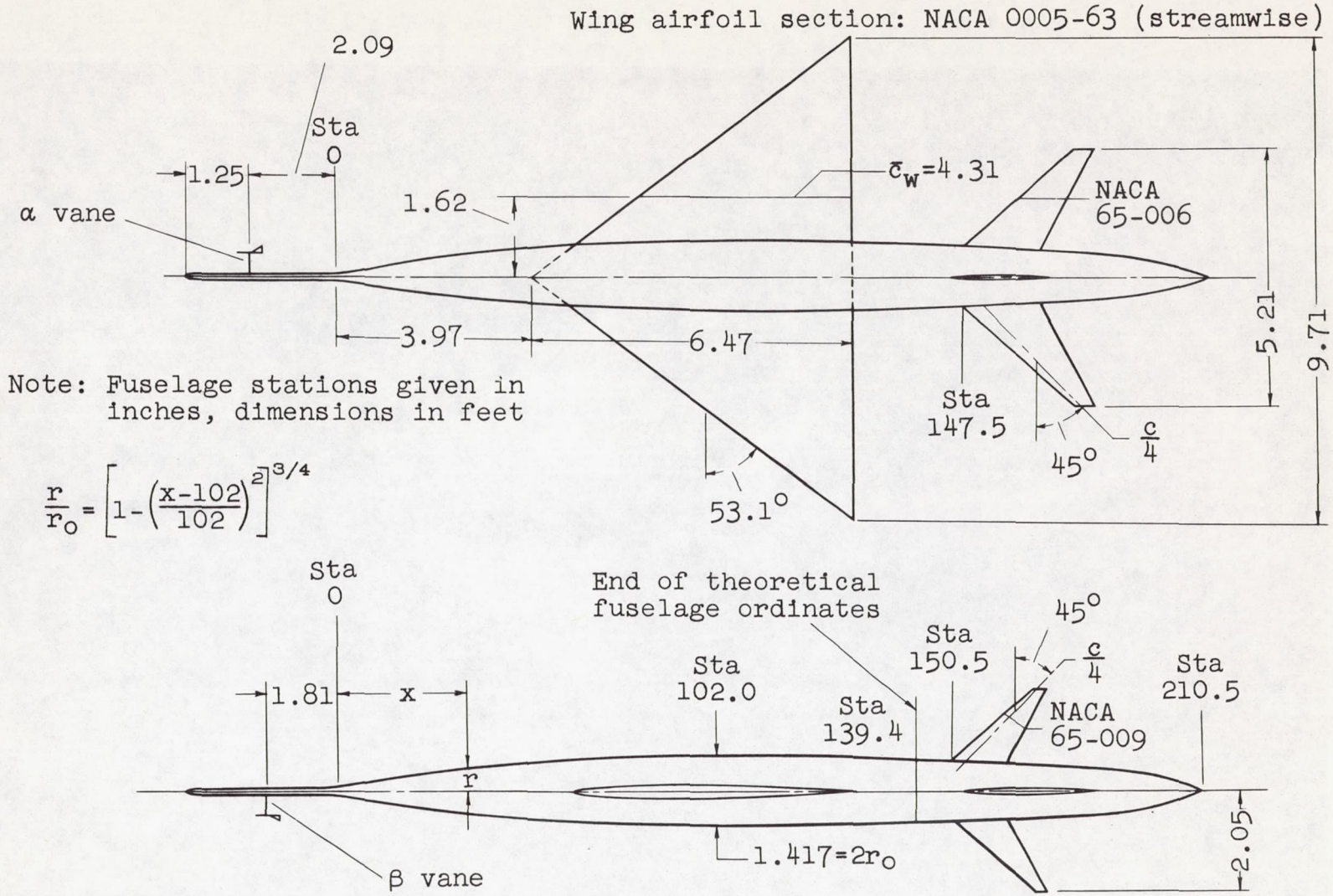

Figure 1.- Dimensional sketch of test model configuration.

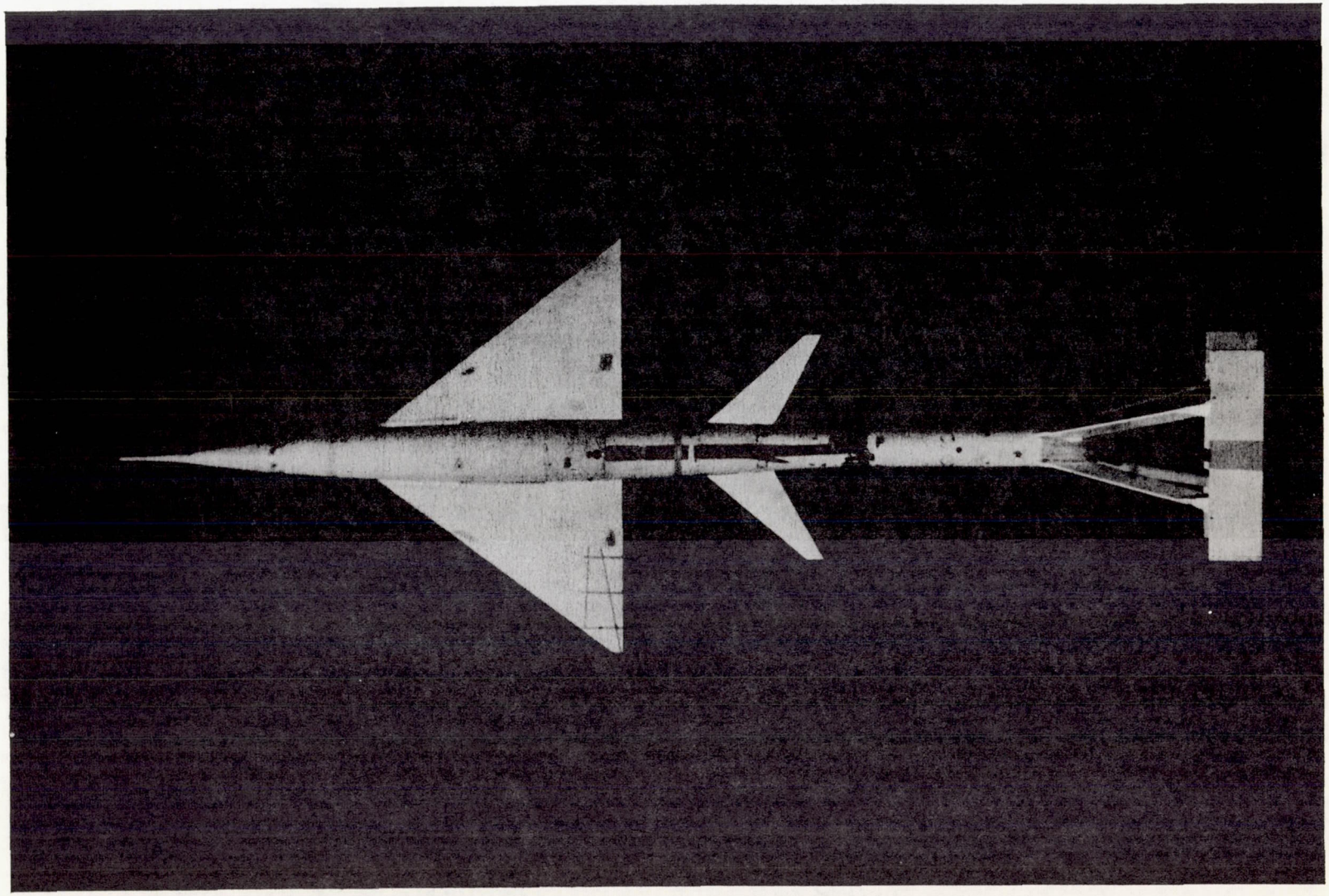

A-19798

Figure 2.- Test model in free flight with booster attached.

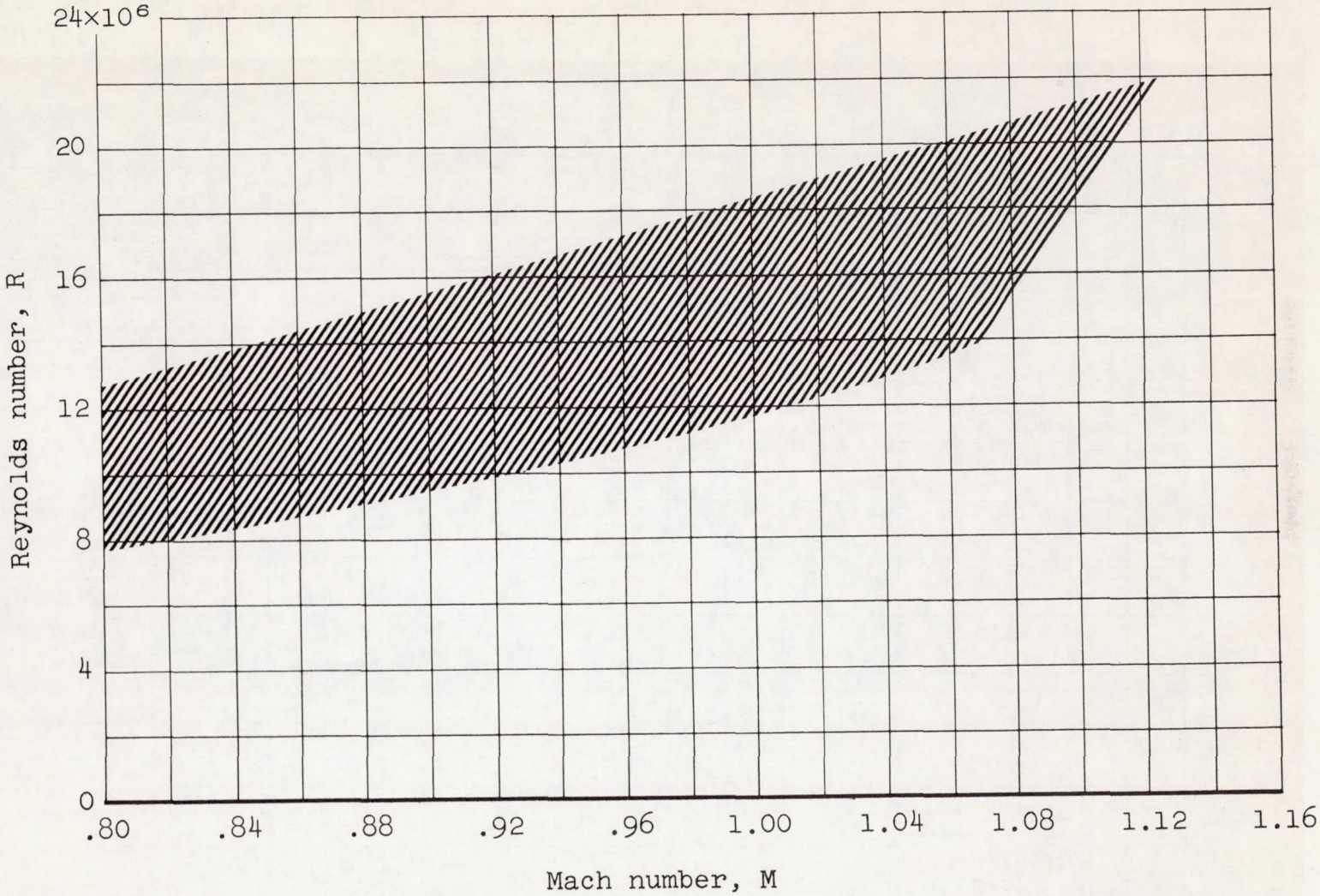

Figure 3.- Variation with Mach number of Reynolds number covered by test program.

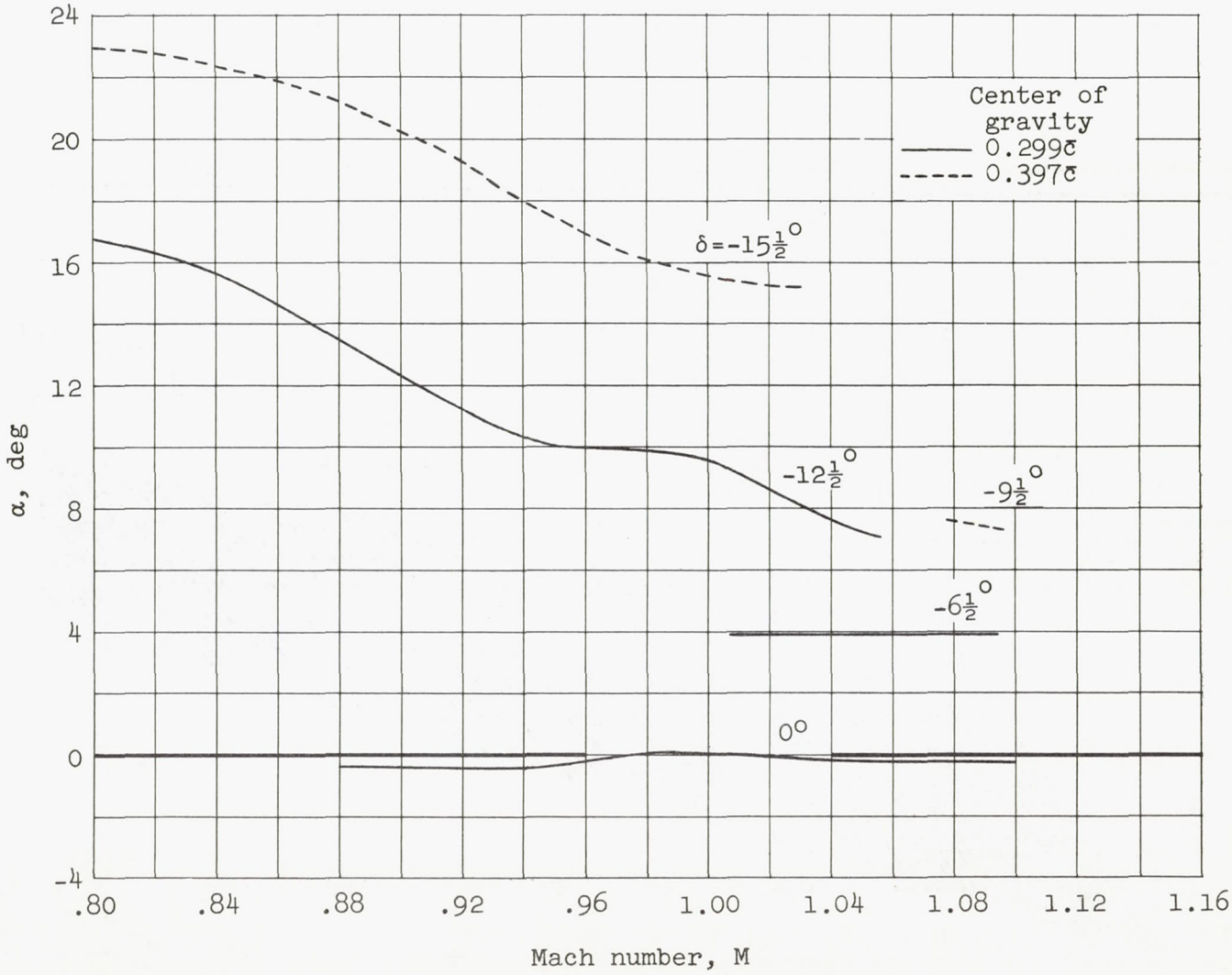

Figure 4.- Variation with Mach number of trim angle of attack for several horizontal-tail settings.

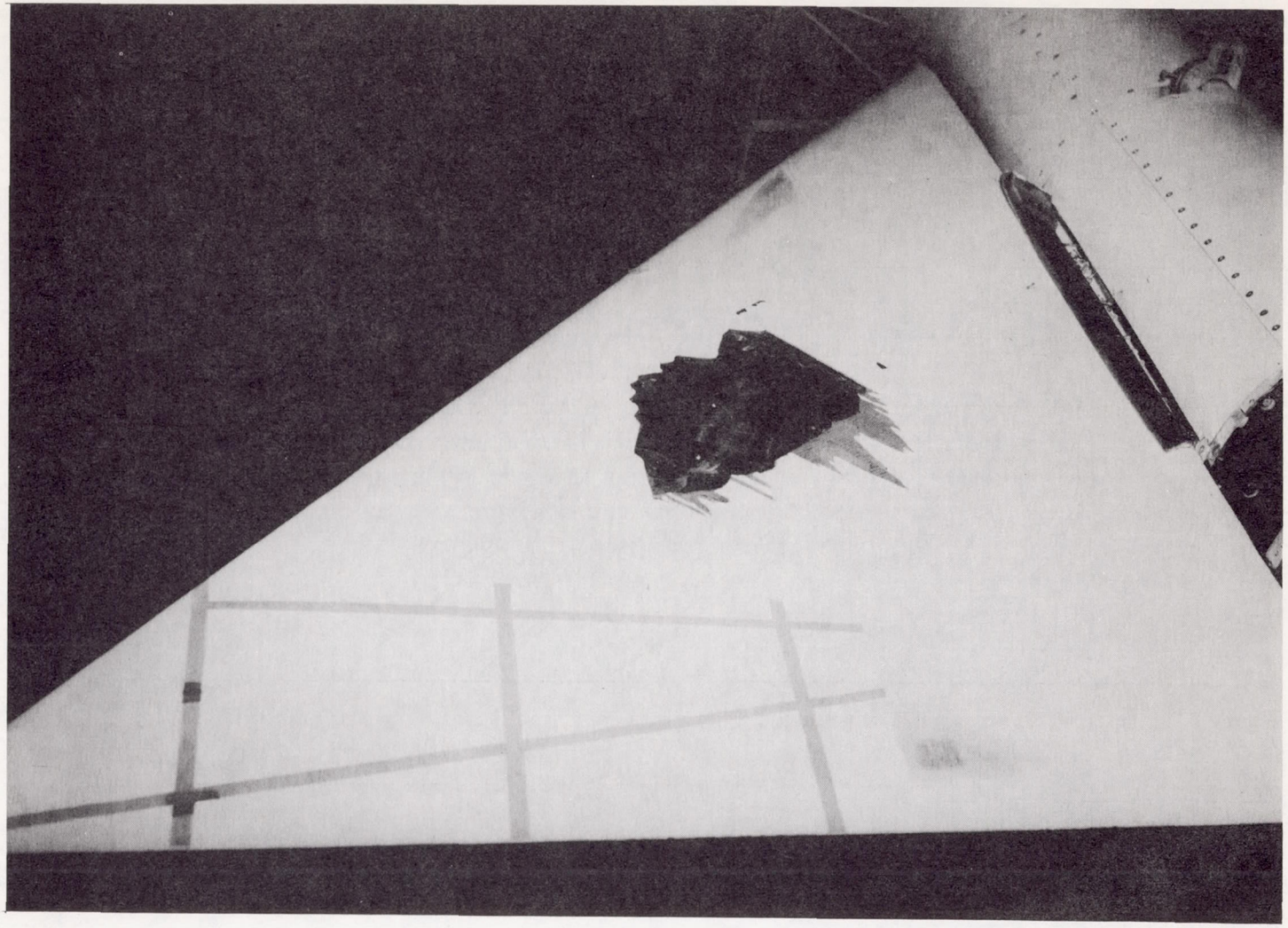

A-19083

Figure 5.- Upper surface of left wing showing damage sustained during drop with $\delta=-12-1/2^{\circ}$.

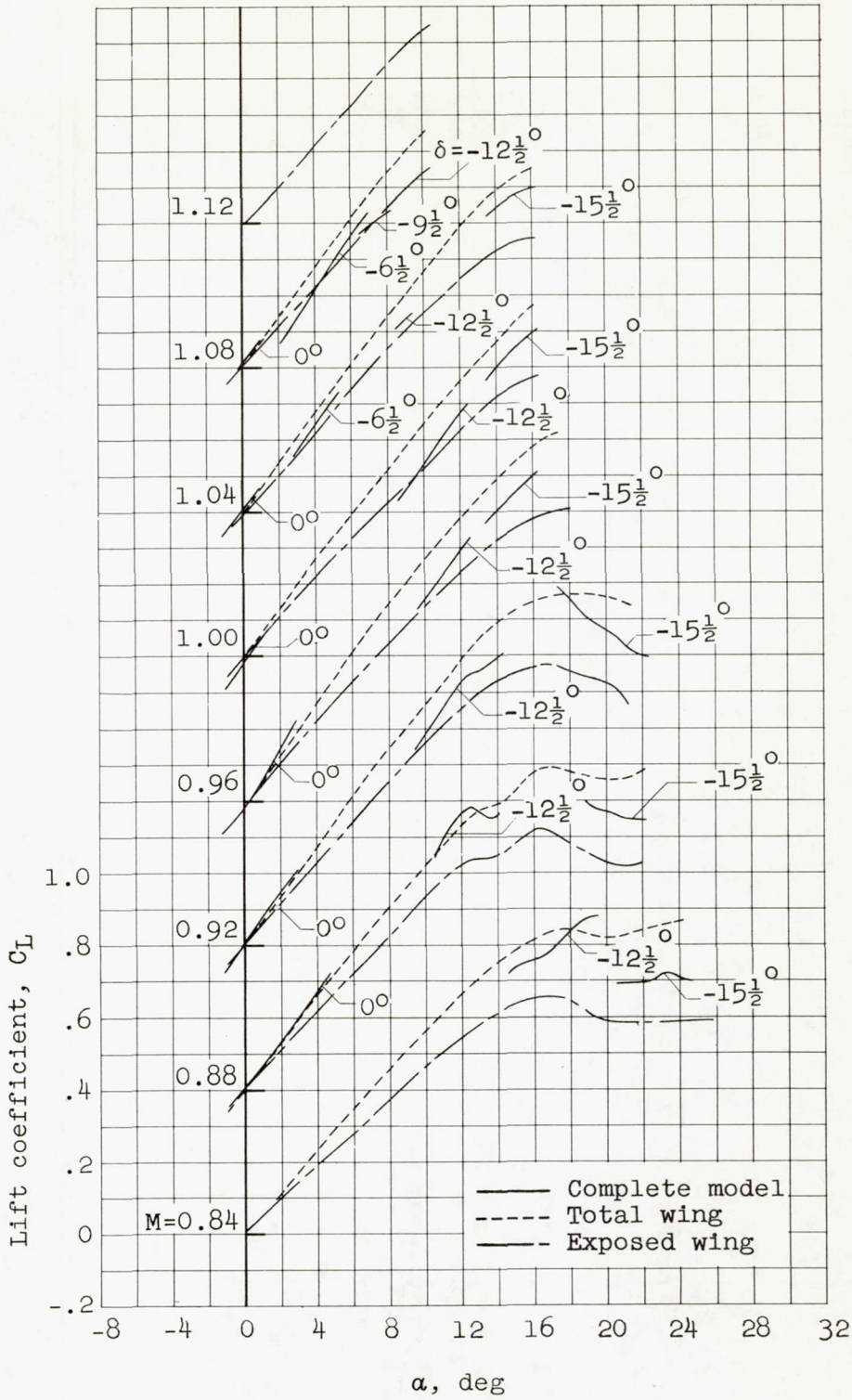

Figure 6.- Lift curves for various components of the test model.

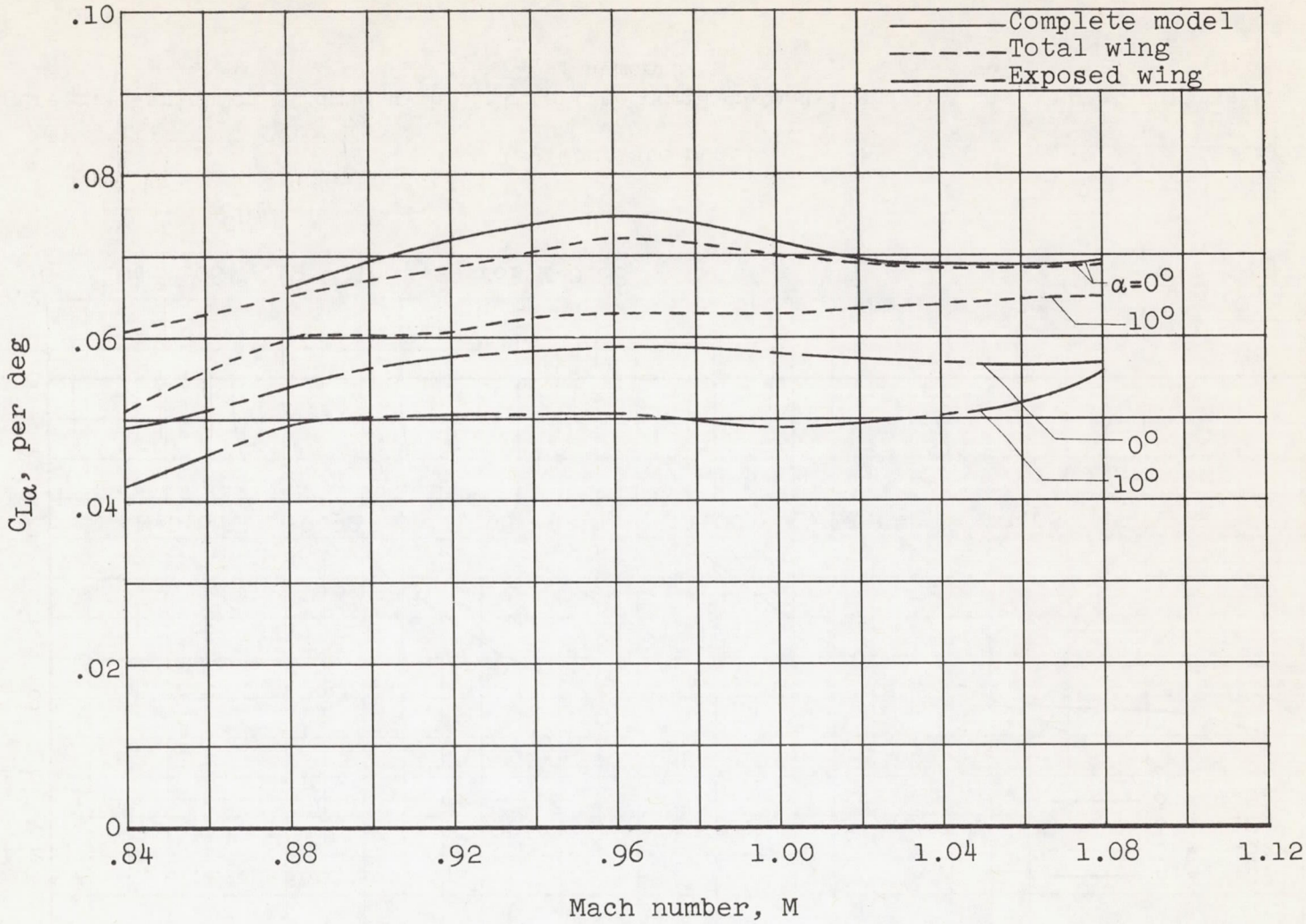

Figure 7.- Variation with Mach number of lift-curve slopes for the components of the test model.

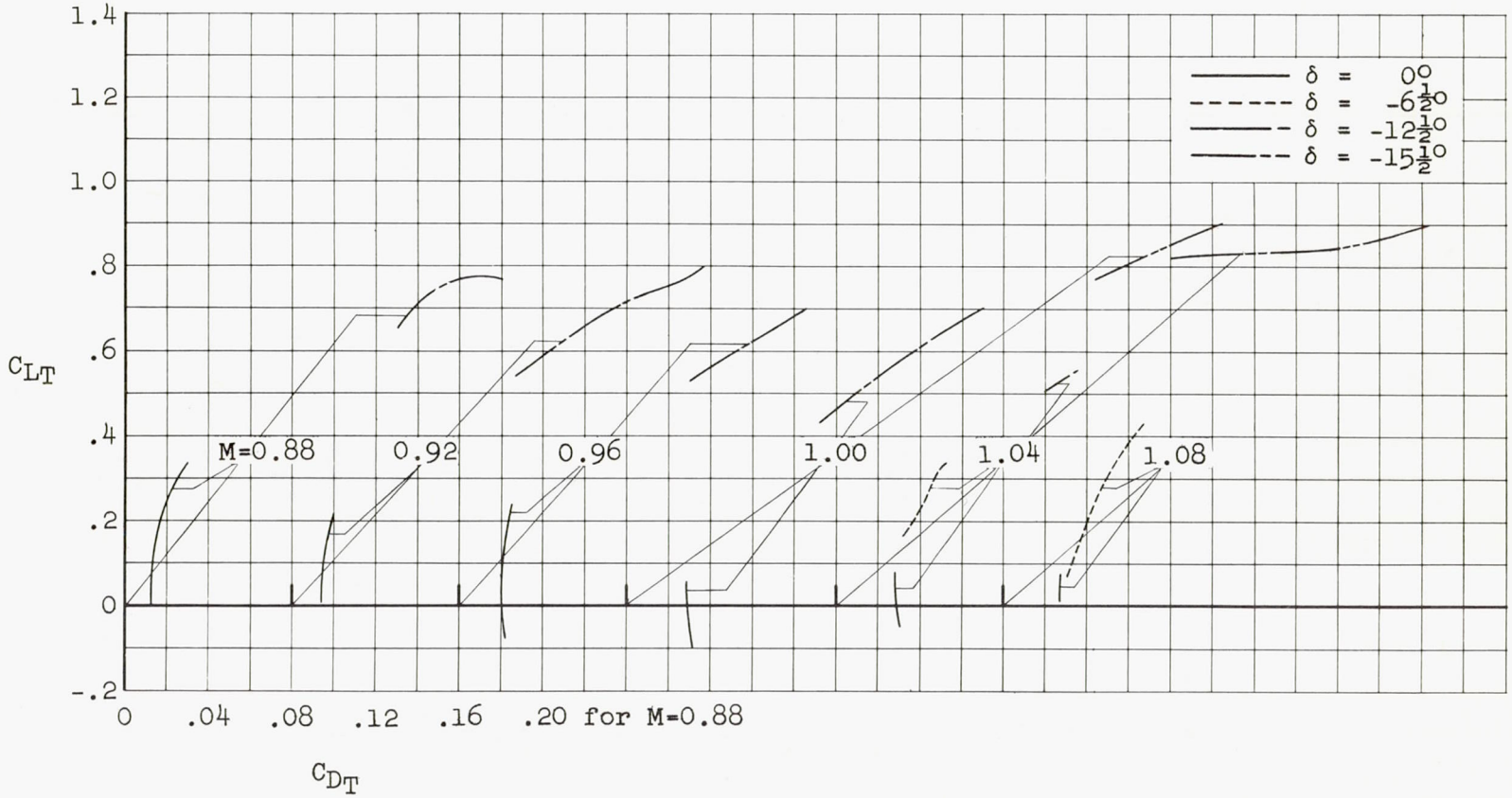

(a) Complete model.

Figure 8.- Variation of drag with lift for the complete model and for the wing at various Mach numbers.

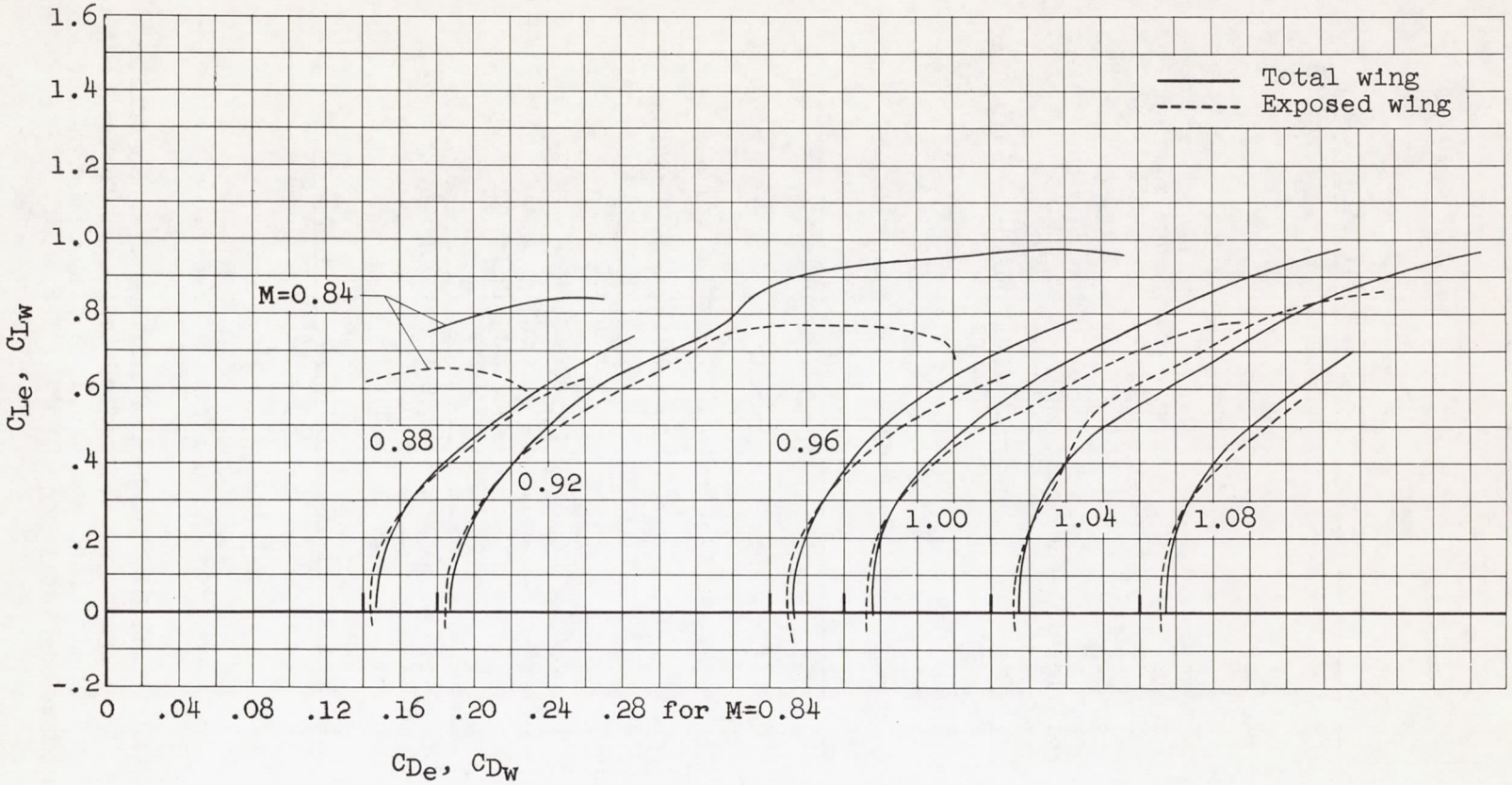

(b) Wing.

Figure 8.- Concluded.

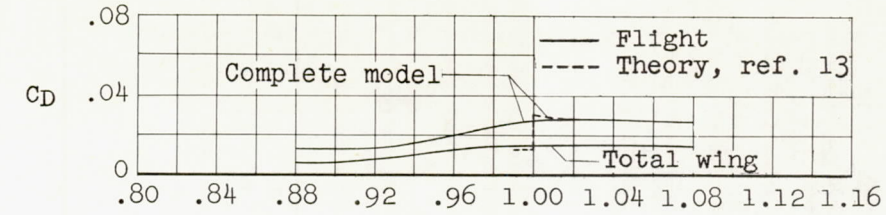

(a) Minimum drag.

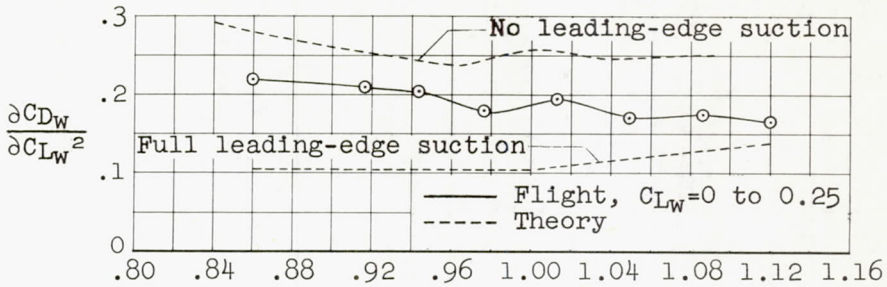

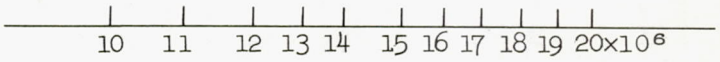

Reynolds number, R_W

(b) Drag rise with lift - total wing.

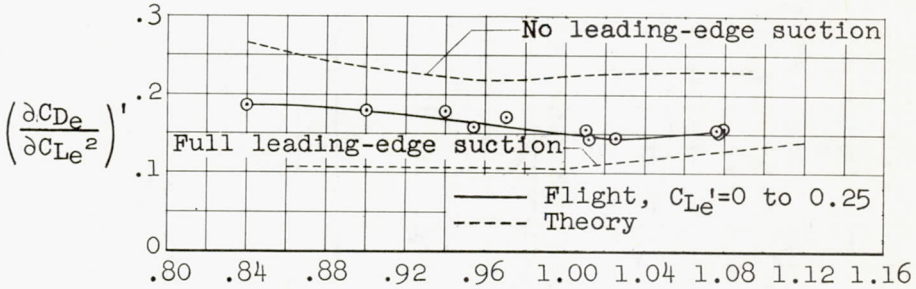

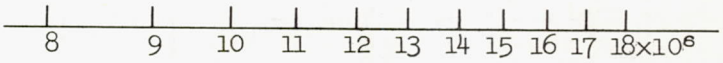

Reynolds number, R_e'

(c) Drag rise with lift - exposed wing.

Figure 9.- Variation with Mach number of minimum drag coefficient for the wing and the complete model, and of drag-rise factor $\partial C_D/\partial C_L^2$ for the wing. Primed values are based on dimensions of the exposed wing, rather than the total wing.

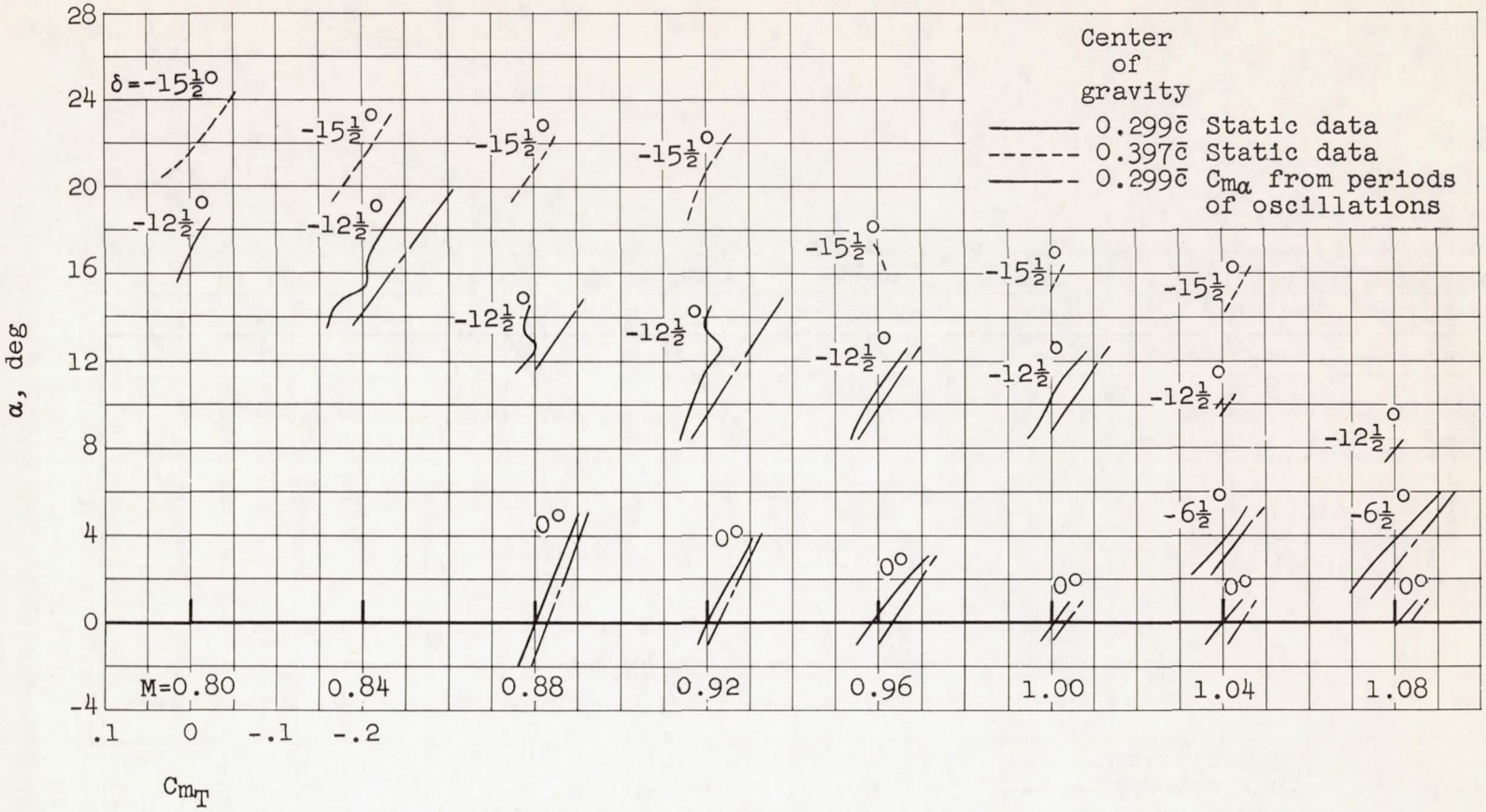

(a) Complete model.

Figure 10.- Variation with angle of attack of pitching-moment coefficients for various components of the test model.

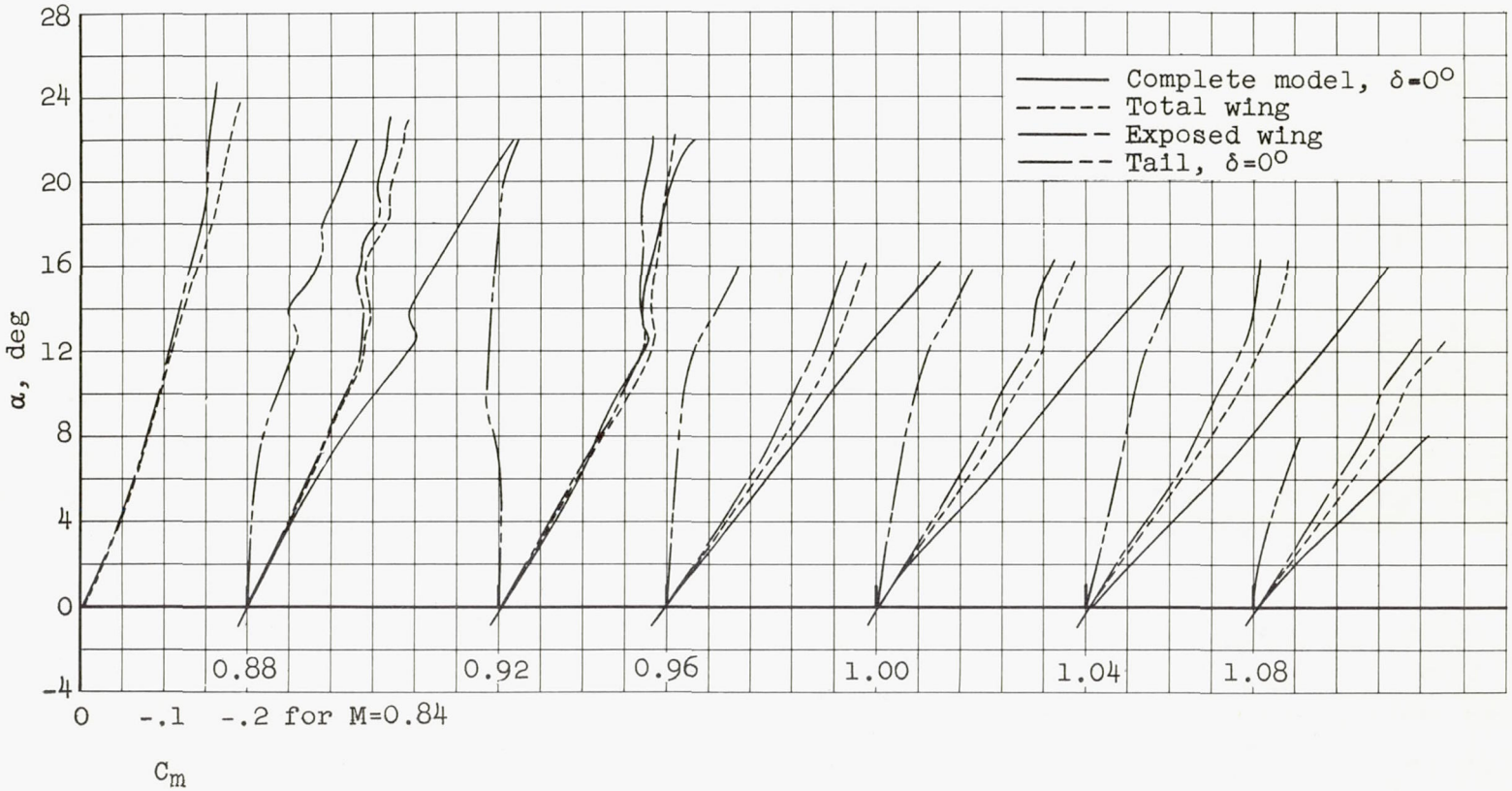

(b) Components of the model; center of gravity at $0.25\bar{c}$.

Figure 10.- Concluded.

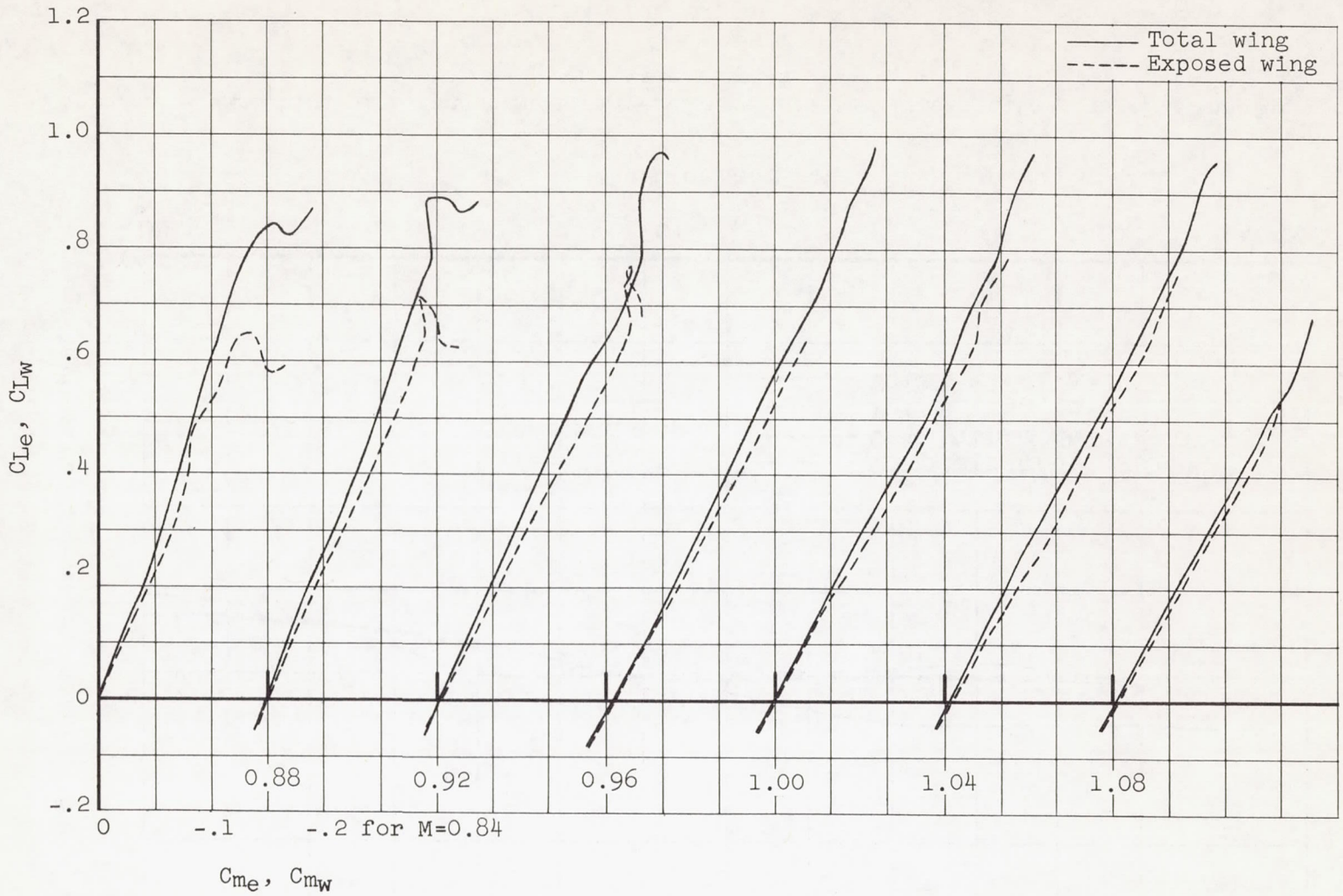

Figure 11.- Variation of pitching-moment coefficient with lift coefficient for wing of model; center of gravity at $0.25\bar{c}$.

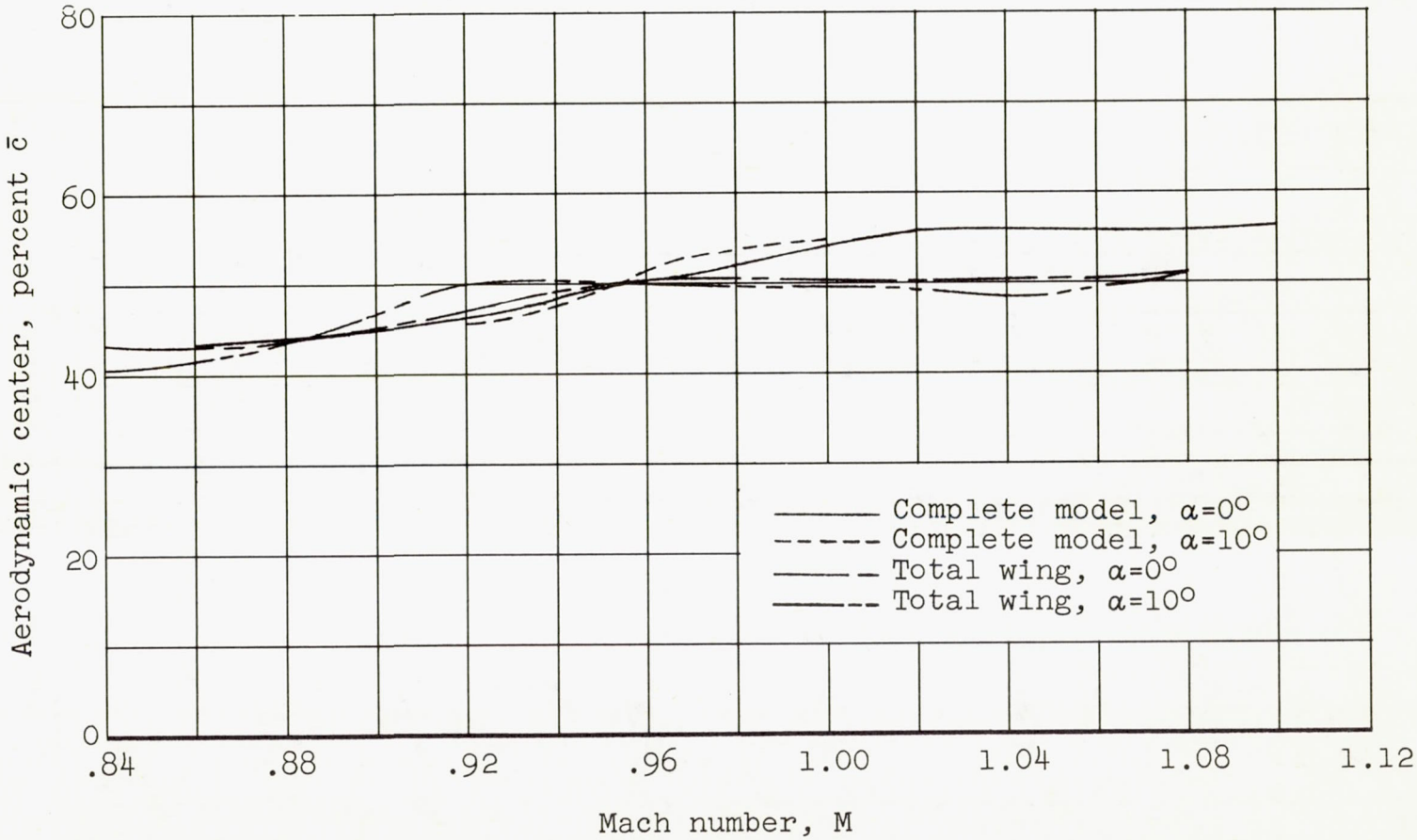

Figure 12.- Variation with Mach number of aerodynamic-center location for the wing and for the complete model.

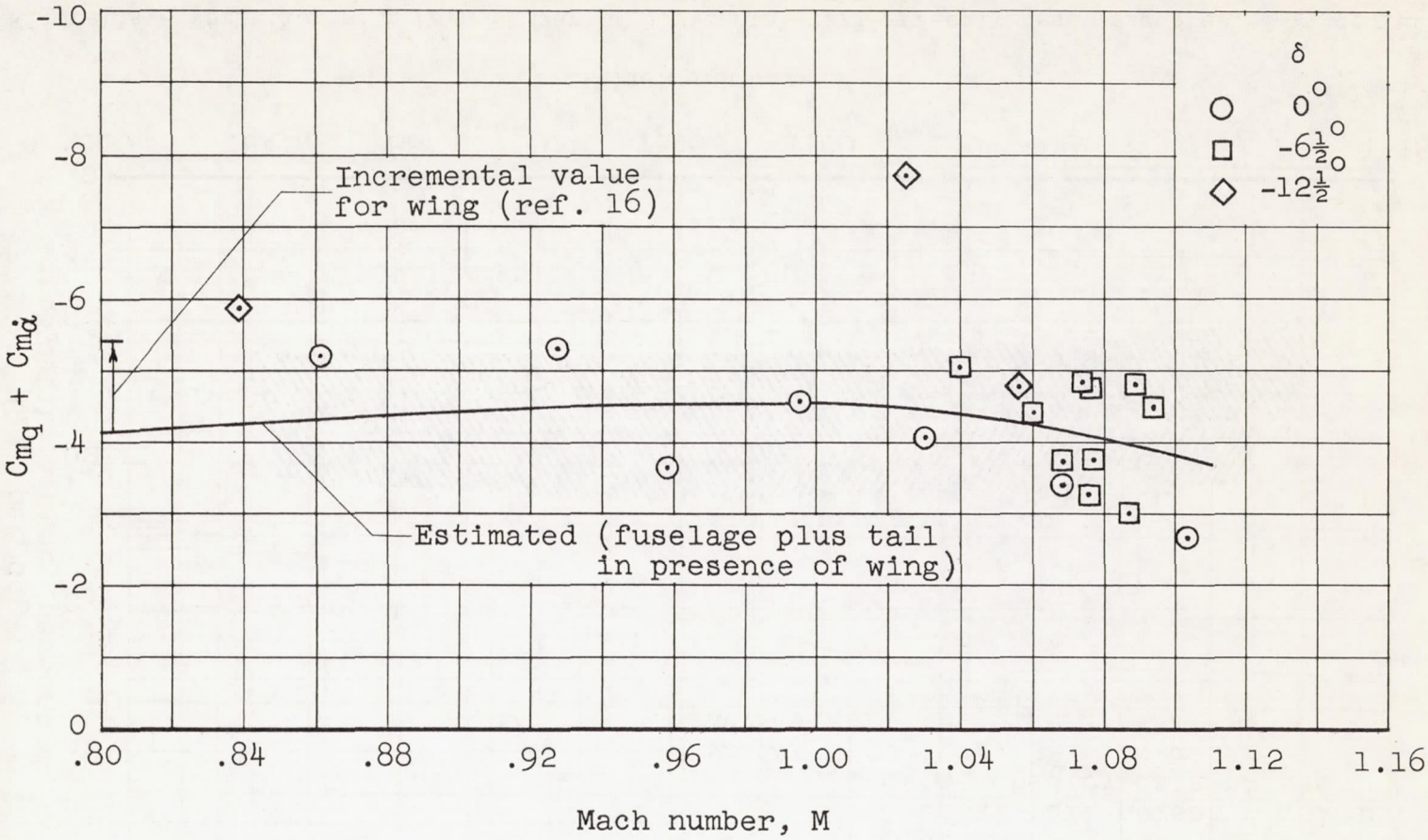

Figure 13.- Variation with Mach number of the damping-in-pitch parameter, $C_{m_q} + C_{m_{\dot{\alpha}}}$.

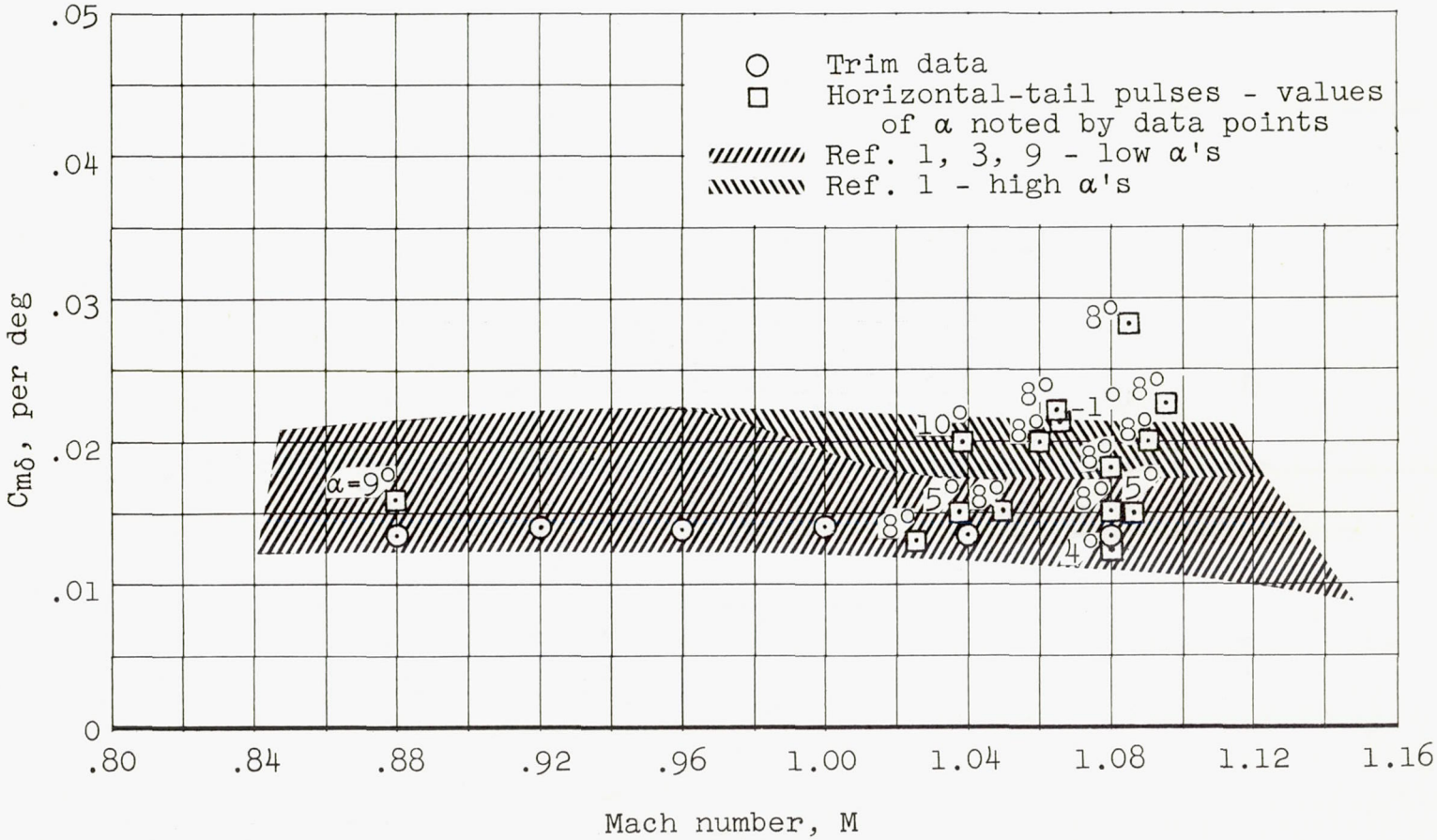

Figure 14.- Variation with Mach number of horizontal-tail-effectiveness parameter, C_{m_δ}; center of gravity at 0.299$\bar{c}$.

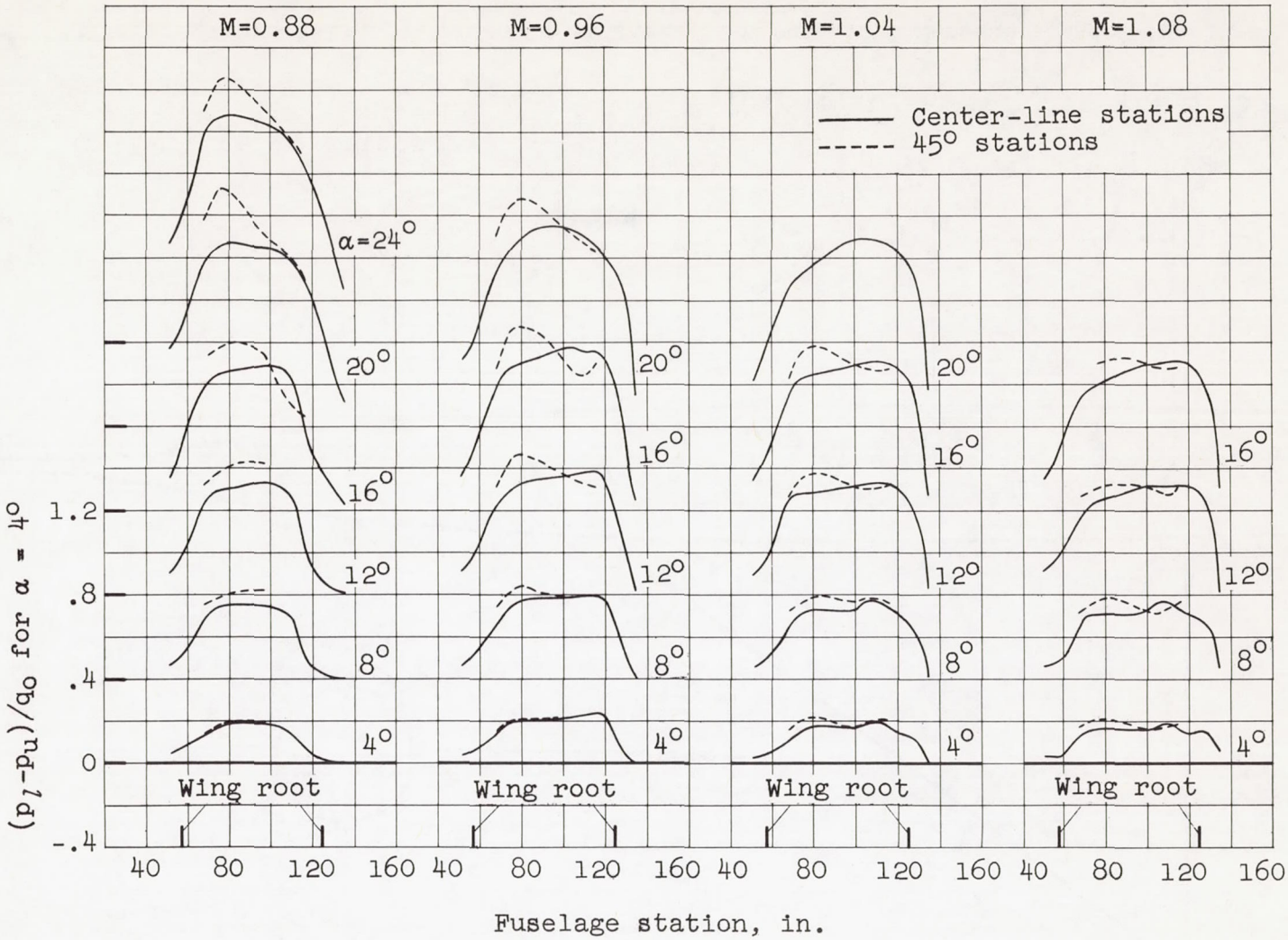

Figure 15.- Loading distribution over the fuselage in the vicinity of the wing.

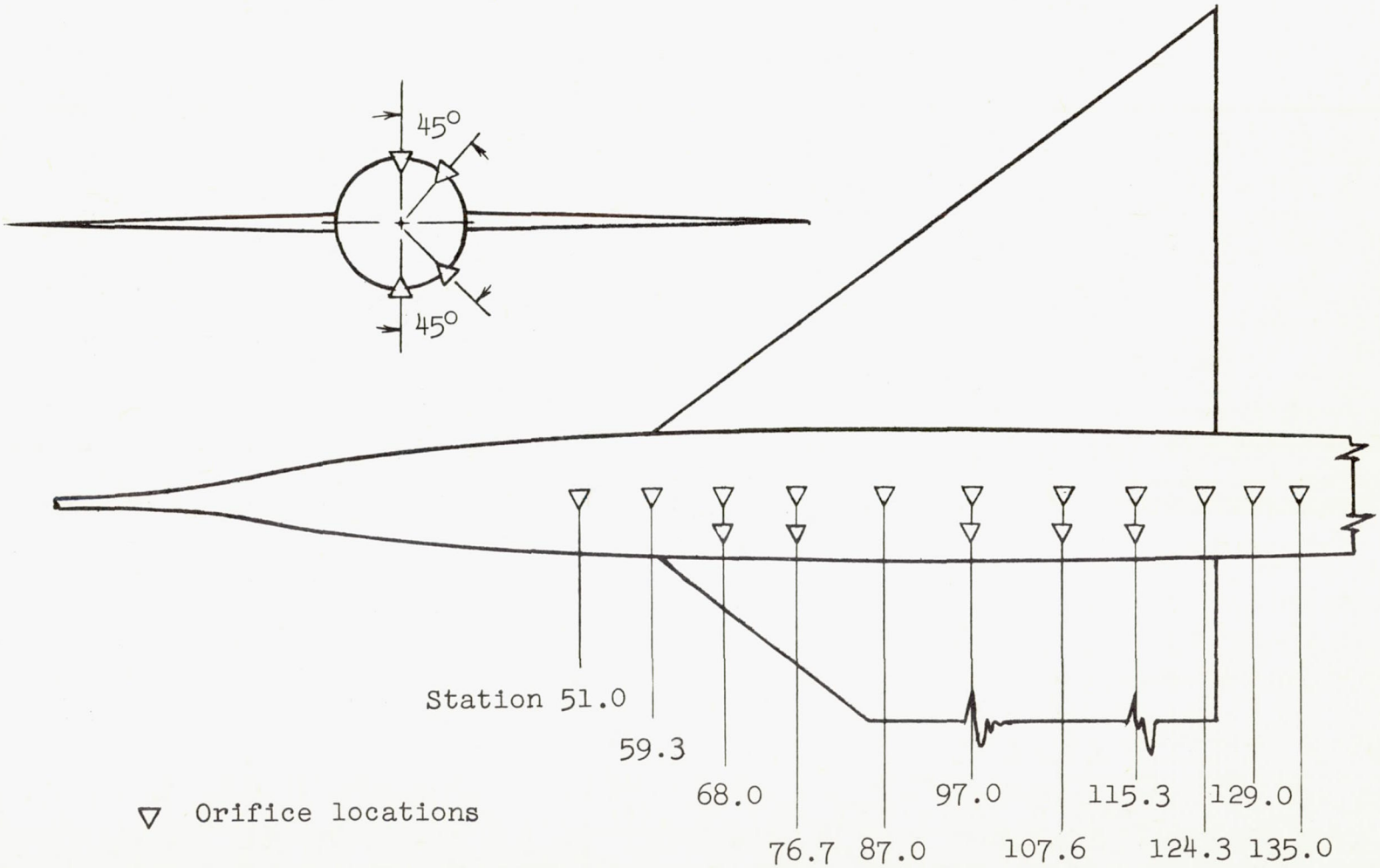

Figure 16.- Locations of pressure orifices in upper and lower surfaces of fuselage.

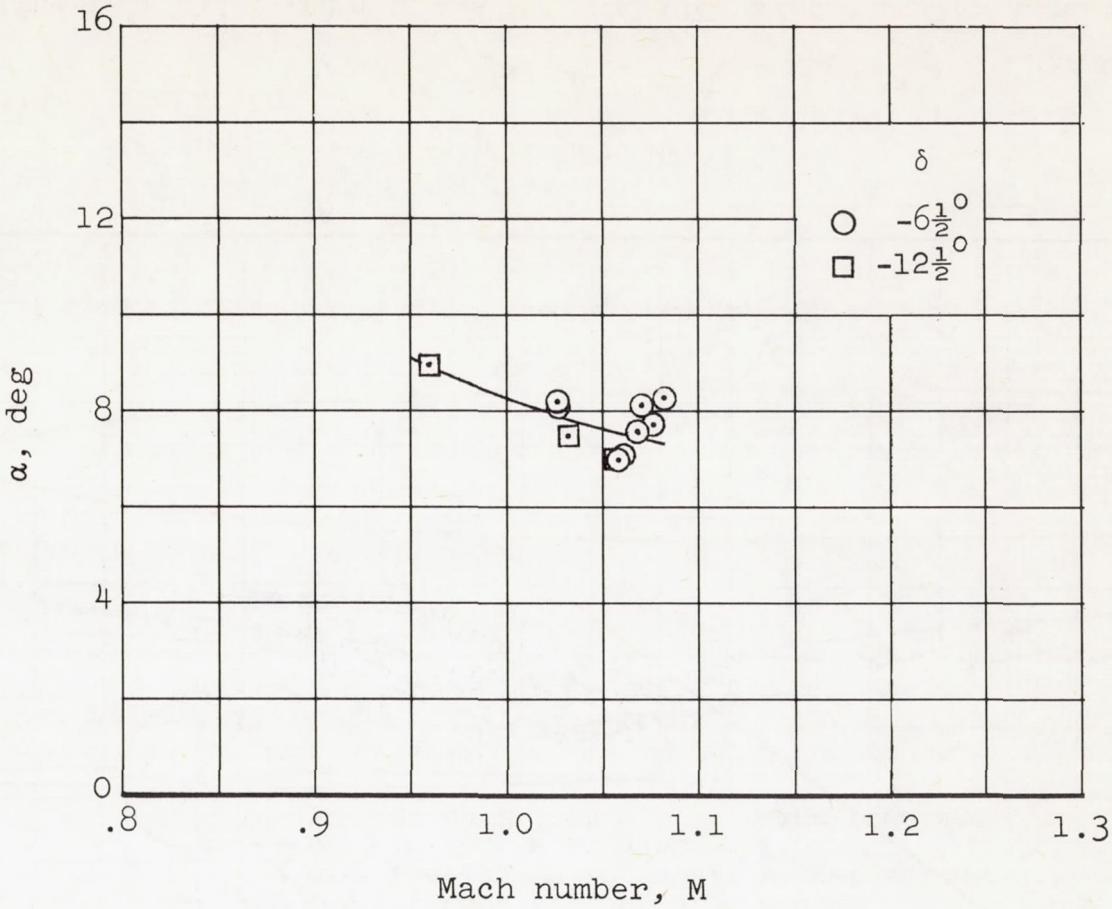

Figure 17.- Variation with Mach number of angle of attack at which buffeting begins.

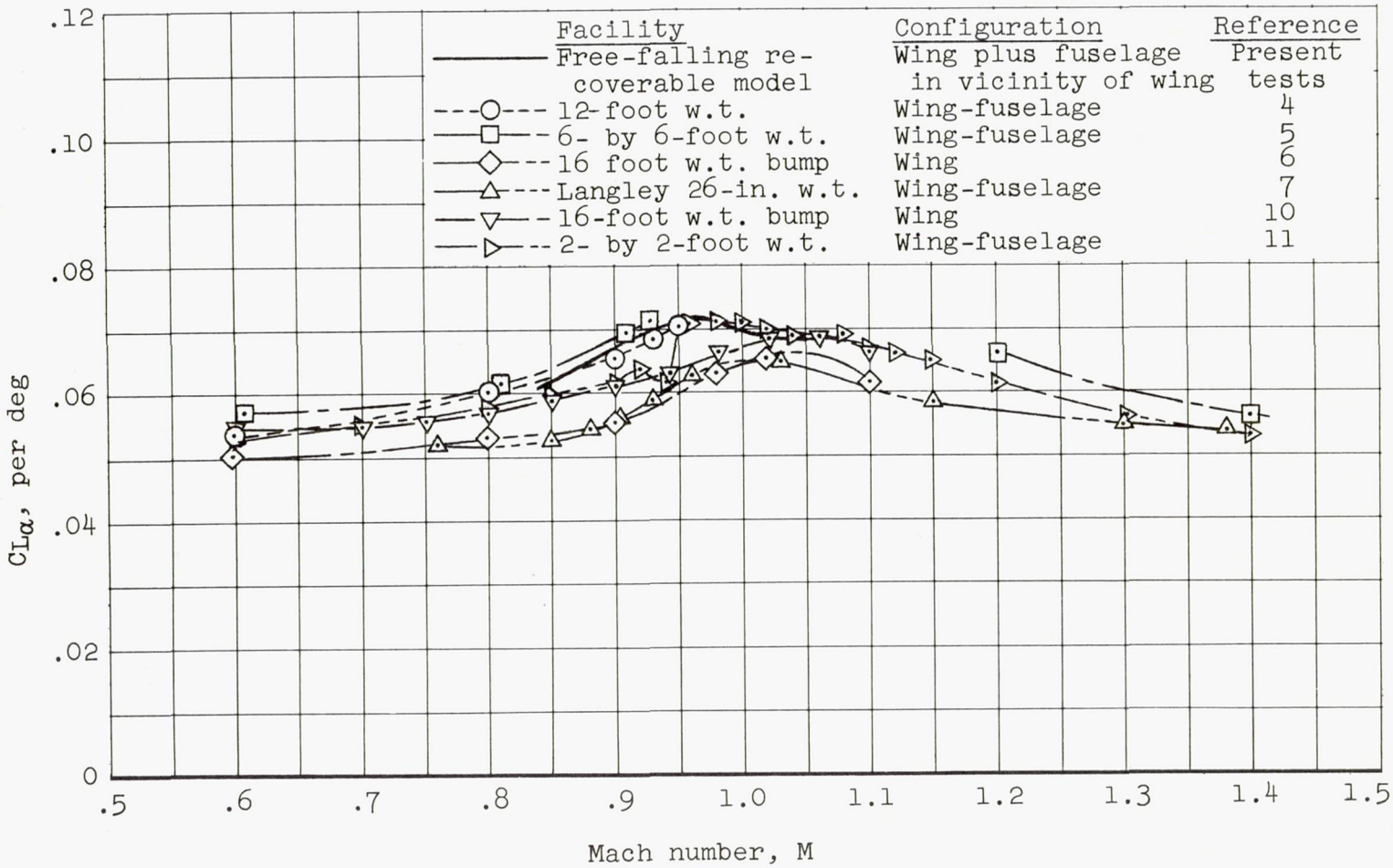

(a) Wing.

Figure 18.- Comparison of lift-curve slopes for total wing and for complete model at zero lift with results obtained from different tests.

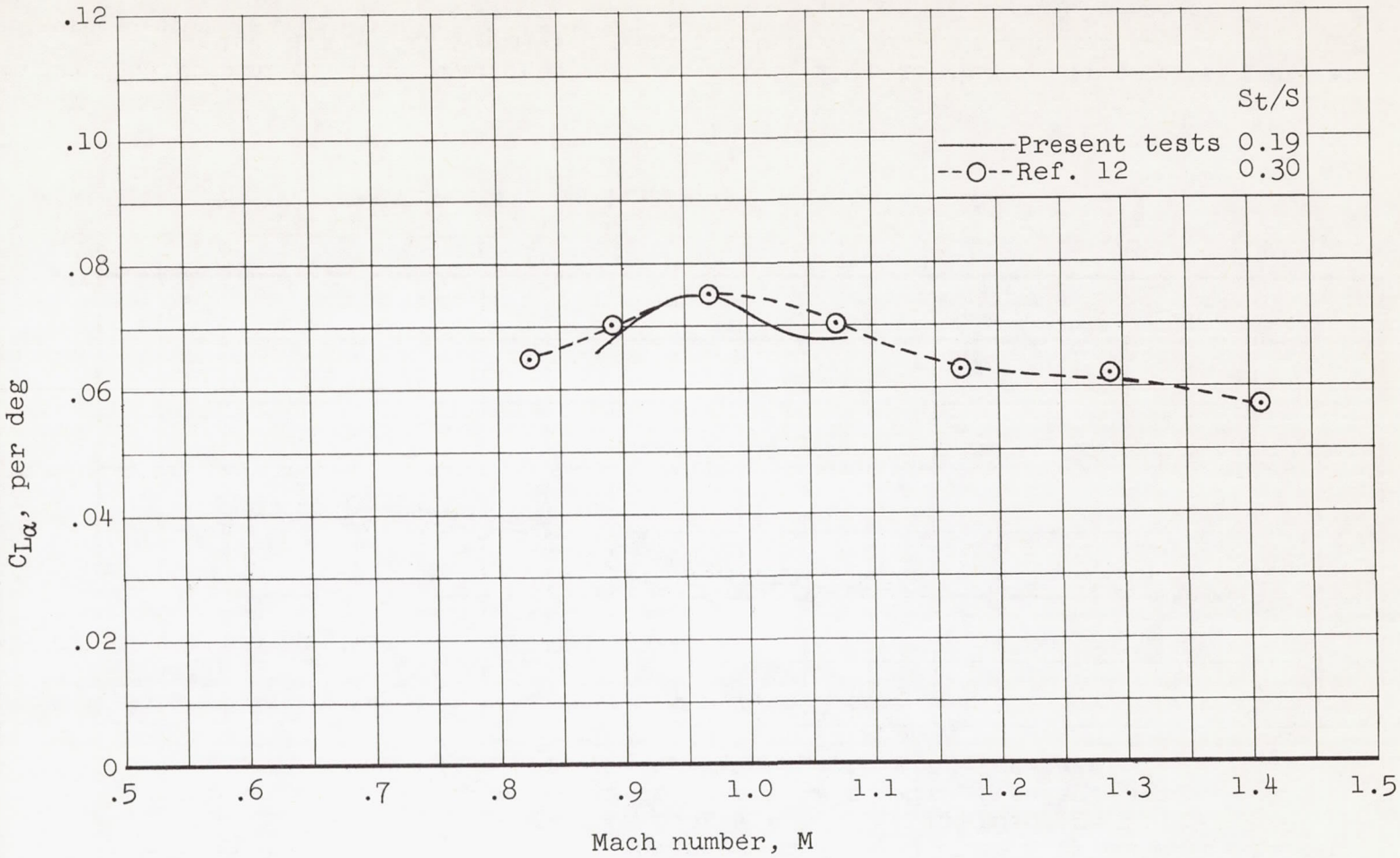

(b) Complete model.

Figure 18.- Concluded.

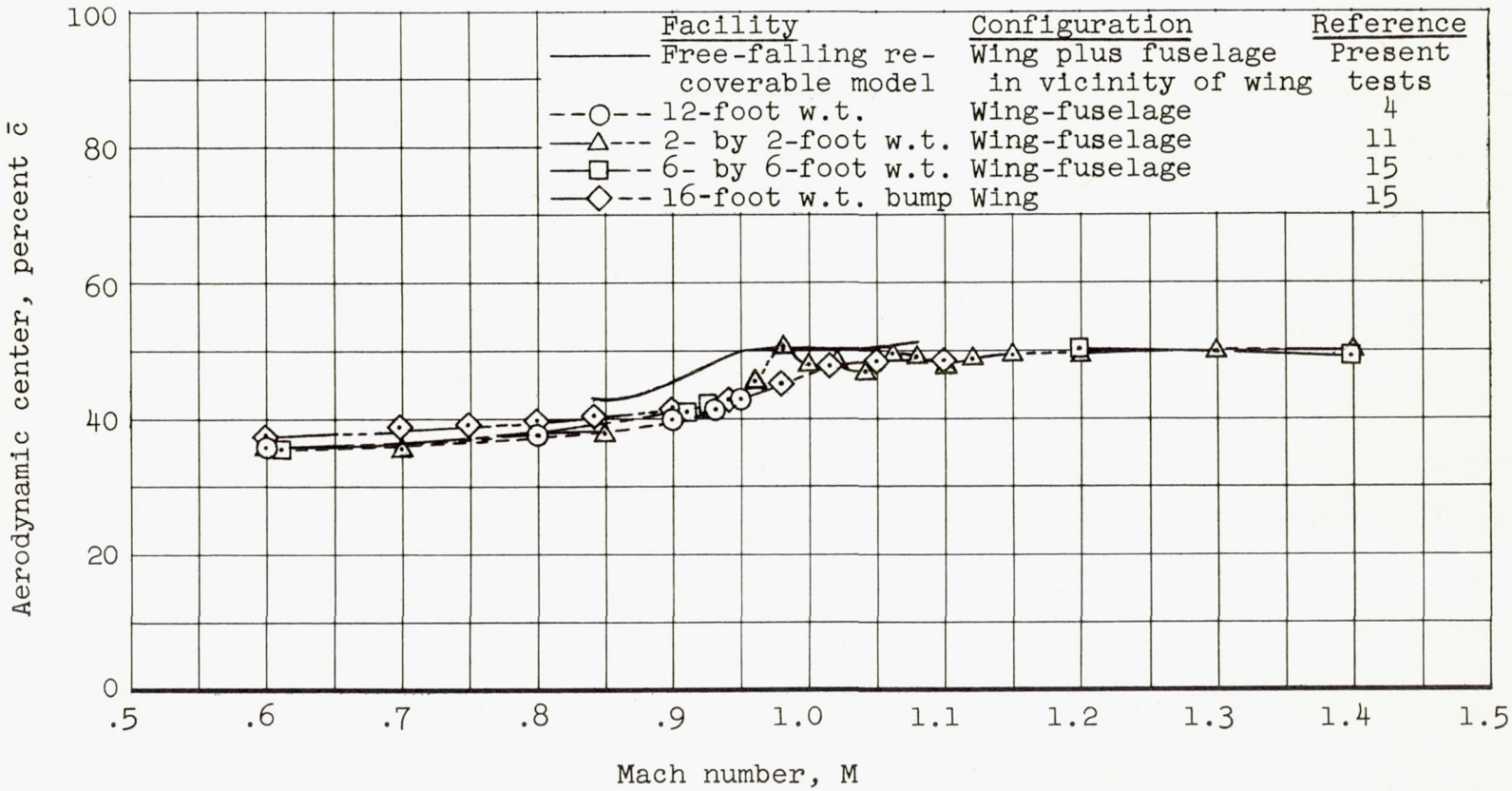

(a) Wing.

Figure 19.- Comparison of aerodynamic-center variations of total wing and of complete model at low lift coefficients with results obtained from different tests.

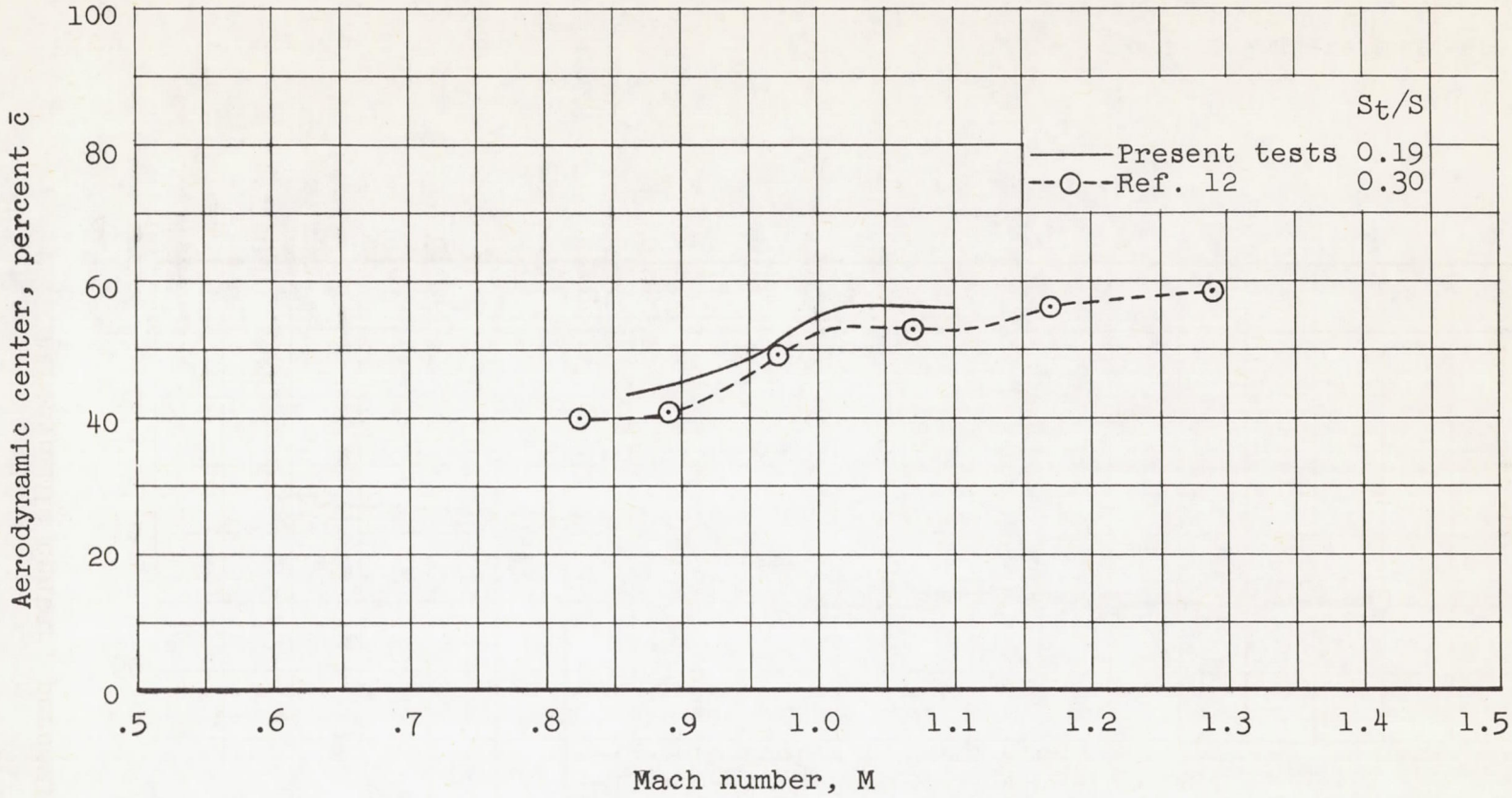

(b) Complete model.

Figure 19.- Concluded.